ISSN 1880-7410

KAYABA TECHNICAL REVIEW

OCT. 2022
No.65

KAYABA TECHNICAL REVIEW No. 65 OCT. 2022

KYB

Our Precision, Your Advantage

KYB Corporation

KYB Corporation

KYB Corporation adopted the common name of KAYABA Corporation on April 1, 2022.

As of August 1, 2022

Head Office World Trade Center Building South Tower 28F, 4-1, Hamamatsu-cyo 2-chome, Minato-ku, Tokyo 105-5128, Japan Tel：(81)3-3435-3511

Basic Technology R&D Center	12-1, Asamizo-dai 1-chome, Minami-ku, Sagamihara-shi, Kanagawa 252-0328, Japan	TEL:(81)42-745-8111
Production Technology R&D Center	60, Dota, Kani-shi, Gifu 509-0206, Japan	TEL:(81)574-26-1453
Developmental Center	1185 Aza-shirasuna, Kashio, Kawabe-cho, Kamo-gun, Gifu 509-0307, Japan	TEL:(81)574-52-1323
Machine Tools Center	60, Dota, Kani-shi, Gifu 509-0206, Japan	TEL:(81)574-26-5310
South Kanto Branch	12-1, Asamizo-dai 1-chome, Minami-ku, Sagamihara-shi, Kanagawa 252-0328, Japan	TEL:(81)42-746-5587
Nagoya Branch	Meieki Nishikibashi Bldg. 2F, 27-13 Meieki 5-chome, Nakamura-ku, Nagoya-shi, Aichi 450-0002, Japan	TEL:(81)52-587-1760
Osaka Branch	2nd TEK Bldg. 3F, 23-20, Esaka-cho 1-chome, Suita-shi, Osaka 564-0063, Japan	TEL:(81)6-6387-3221
Fukuoka Branch	Yasukawa-Sangyo Bldg. 5F, 6-26, Hakataeki-higashi 2-chome, Hakata-ku, Fukuoka-shi, Fukuoka, 812-0013, Japan	TEL:(81)92-411-2066
Hiroshima Sales Office	Hiroshima Bldg. 4F, 12-16, Hikari-machi 1-chome, Higashi-ku, Hiroshima-shi, Hiroshima, 732-0052, Japan	TEL:(81)82-567-9166
SAGAMI PLANT	12-1 Asamizo-dai 1-chome, Minami-ku, Sagamihara-shi, Kanagawa 252-0328, Japan	TEL:(81)42-746-5511
KUMAGAYA PLANT	2050, Nagazaike, Fukaya-shi, Saitama 369-1193, Japan	TEL:(81)48-583-2341
GIFU NORTH PLANT	2548, Dota, Kani-shi, Gifu 509-0298, Japan	TEL:(81)574-26-5111
GIFU SOUTH PLANT	505, Dota, Kani-shi, Gifu 509-0297, Japan	TEL:(81)574-26-1111
GIFU EAST PLANT	60, Dota, Kani-shi, Gifu 509-0206, Japan	TEL:(81)574-26-2135
MIE PLANT	1129-11, Kumozunagatsune-cho, Tsu-shi, Mie 514-0396, Japan	TEL:(81)59-234-4111
KYB-CS Co., Ltd.	1129-11, Kumozunagatsune-cho, Tsu-shi, Mie 514-0396, Japan	TEL:(81)59-234-9260
KYB TRONDULE Co., Ltd.	3909, Ura, Nagaoka-shi, Niigata, 949-5406, Japan	TEL:(81)258-92-6903
TAKAKO Industries, INC.	32-1 Housono-Nishi 1-chome, Seika-cho, Souraku-gun, Kyoto, 619-0240, Japan	TEL:(81)774-95-3336
KYB Kanayama Co., Ltd.	4350-130, Aza-Funeno Tobe, Kanayama-cho, Gero-shi, Gifu, 509-1605, Japan	TEL:(81)576-35-2201
KYB-YS Co., Ltd.	9165 Sakaki, Sakaki-machi, Hanishina-gun, Nagano, 389-0688, Japan	TEL:(81)268-82-2850
KYB Motorcycle Suspension Co., Ltd.	509, Dota, Kani-shi, Gifu 509-0298, Japan	TEL:(81)574-27-1170
KYB Logistics Co., Ltd.	2-16, Himegaoka, Kani-shi, Gifu 509-0249, Japan	TEL:(81)574-26-6427
JAPAN ANALYSTS Co., Ltd.	KYB Corporation SAGAMI PLANT 1-12-1, Asamizodai, Minami-ku, Sagamihara-shi, Kanagawa 252-0328, Japan	TEL:(81)42-749-7512
Kensiyuu Co., Ltd.	2-8-4, Bijogi kita, Toda-shi, Saitama 335-0038, Japan	TEL:(81)48-499-9336

Overseas Subsidiaries and Affiliates

[Americas]

KYB Americas Corporation
2625 North Morton, Franklin, Indiana 46131, U.S.A.
TEL: (1)317-736-7774

Takako America Co., Inc.
715 Corey Road Hutchinson, Kansas 67504-1642, U.S.A.
TEL: (1)620-663-1790

KYB International America, Inc.
2625 North Morton, Franklin, Indiana 46131, U.S.A.
TEL: (1)317-346-6719

KYB Mexico S.A. de C.V.
Circuito San Roque Norte #300 Santa Fe II, Puerto Interior, Silao Guanajuato, CP 36275, Mexico
TEL: (52)472-748-5000

KYB Manufacturing do Brasil Fabricante de Autopeças S.A.
Rua Francisco Ferreira da Cruz, 3000, Fazenda Rio Grande-Parana, CEP 83820-293, Brazil
TEL: (55)-41-2102-8200

Comercial de AutopeÇas KYB do Brasil Ltda.
Rua Cyro Correia Pereira, 2400 Suite 07-Cidade Industrial, Curitiba-PR, 81460-050, Brazil
TEL: (55)41-3012-3620

[Europe]

KYB Europe GmbH
Margaretha-Ley-Ring 2, 85609 Aschheim, Germany
TEL: (49)-89-5480188-0

KYB Suspensions Europe, S.A.U.
Ctra, Irurzun S/No, 31171 Ororbia Navarra, Spain
TEL: (34)948-421700

KYB Advanced Manufacturing Spain, S.A.U.
Poligono Industrial Perguita Calle B, No. 15, 31210 Los Arcos Navarra, Spain
TEL: (34)948-640336

KYB Manufacturing Czech, s.r.o.
U Panasonicu 277, Stare Civice, 530 06 Pardubice, Czech Republic
TEL: (420)466-812-233

KYB CHITA Manufacturing Europe s.r.o.
Prumyslova 1421, 53701 Chrudim, Czech Republic
TEL: (420)469-363-302

LLC KYB Eurasia
117638 Odesskaya street 2 building A, Moscow, Russian Federation
TEL: (7)495-7716010

[Asia]

KYB Steering (Thailand) Co., Ltd.
700/829 Moo 6, T. Nongtamlueng Amphur Panthong, Chonburi 20160,Thailand
TEL: (66)3-818-5559

KYB(Thailand)Co., Ltd.
700/363 Moo 6, Amata Nakorn Industrial Park2, Bangna-Trad Road, K.M. 57, Tambol Don Hua Roh, Amqhur Muang, Chonburi 20000, Thailand
TEL: (66)3-846-9999

KYB Asian Pacific Corporation Ltd.
No. 4345 Bhiraj Tower at BITEC, Unit 1209-1211, 12th Floor, Sukhumvit Road, Bangnatai Sub-District, Bangna District, Bangkok 10260, Thailand
TEL: (66)2-300-9777

KYB-UMW Malaysia Sdn. Bhd.
Lot 8, Jalan Waja 16, 42500 Telok Panglima Garamg, Kuala Langat, Selangor, Malaysia
TEL: (60)3-3322-0800

PT. KYB Hydraulics Manufacturing Indonesia
JL. Irian X blok RR2 Kawasan Industri MM2100, Cikarang Barat 17520, Indonesia
TEL: (62)21-28080145

PT. Kayaba Indonesia
JL, Jawa Blok ii No. 4 Kawasan Industri MM2100, Cikarang Barat 17520, Indonesia
TEL: (62)21-8981456

PT. Chita Indonesia
JL, Jawa Blok ii No. 4 Kawasan Industri MM2100, Cikarang Barat 17520, Indonesia
TEL: (62)21-89983737

KYB Manufacturing Vietnam Co., Ltd.
Plot I 10-I 11-I 12, Thang Long Industrial Park, Vong La, Dong Anh District, Hanoi, Vietnam
TEL: (84)24-3881-2773

Takako Vietnam Co., Ltd.
27 Dai Lo Doc Lap, Vietnam Singapore Industrial Park, Thuan An District, Binh Duong, Vietnam
TEL: (84)274-378-2954

永華機械工業股份有限公司
KYB Manufacturing Taiwan Co., Ltd.
No. 493, Guang Hsing Road, Bade District, Taoyuan City, 33454, Taiwan
TEL: (886)3-368-3123

KYB Motorcycle Suspension India Pvt. Ltd.
Pilot No. 6, Sipcot Industrial Park, Vallam Vadagal Village, Sriperumbudur Taluk, Kancheepuram District 631604 Tamil Nadu, India
TEL: (91)44-3012-4301

KYB-Conmat Pvt. Ltd.
702-703, Beside N. H. No. 8, Por, Vadodara 391243, Gujatat, India
TEL: (91)960-1551608

KYB Corporation Chennai Branch
No. 408, Height 1, Temple Green Project, Mathur Village, Sriperumbudur Taluk, Kancheepuram District, India 602105
TEL: (91)2568-0501

【China】

凱迩必(中国)投資有限公司
KYB (China) Investment Co., Ltd.
No.99, Xiyun Road, Dingmao, Zhenjiang New Zone, Zhenjiang, Jiangsu, 212009, China
TEL: (86)511-8558-0300

凱迩必機械工業(鎮江)有限公司
KYB Industrial Machinery (Zhenjiang) Ltd.
No.98, Xiyun Road, Dingmao, Zhenjiang New Zone, Zhenjiang, Jiangsu, 212009, China
TEL: (86)511-8889-1008

無錫凱迩必拓普減震器有限公司
Wuxi KYB Top Absorber Co., Ltd.
No. 2 Xikun North Road, Singapore Industrial Zone, Xinwu District, Wuxi, Jiangsu, 214028, China
TEL: (86)510-8528-0118

常州朗鋭凱迩必減振技術有限公司
Changzhou KYB Leadrun Vibration Reduction Technology Co., Ltd.
No. 19 Shunyuan Road, New District, Changzhou, Jiangsu 213125 China
TEL: (86)519-8595-7206

湖北恒隆凱迩必汽車電動転向系統有限公司
Hubei Henglong & KYB Automobile Electric Steering System Co., Ltd.
108 Shacen Road, Economic and Technological Development Zone, Jingzhou, Hubei, China. 434000
TEL: (86)716-416-7951

知多弾簧工業(鎮江)有限公司
CHITA KYB Manufacturing (Zhenjiang) Co., Ltd.
No. 8 Building-1F, New Energy Industrial Park (North Park), No. 300, Gangnan Road, Zhenjiang New District, Jiangsu 212132, China
TEL: (86)511-8317-2570

KAYABA TECHNICAL REVIEW

No. 65 OCT. 2022

CONTENTS

Foreword

Rethink of Hydraulics for Sustainable Robotics

HYON Sang Ho*

1. Prolog: Meditation During COVID-19 Pandemic

Two years ago, when the world was first hit by COVID-19 infections, I tried to think of the value of robots. I finally concluded that robots are ultimately a tool for mass production, rather than machinery that can help people. I have a university class on Robot Motion Control to teach students textbook theories for high-speed and accurate control of hand motion trajectory tracking. This is essentially robotic theory for mass production. Today, however, the world is saying "No" to mass production or volume consumption.

When our socioeconomic activities were substantially curbed by the COVID-19 pandemic, people fully realized how their individual activities should be prioritized or how many so-called "bullshit jobs" they had. While I was teaching online via my PC screen at home feeling something was wrong, essential workers throughout the world were being exposed to risks of the infection as they diligently worked to relentlessly support society.

We may now have grown more or less accustomed to the pandemic situation. Looking around, we can find roads, waterworks, power grids, and other society supporting infrastructure having seriously deteriorated due to a lack of labor. Infrastructure is something that is man-made. If you say people's health can be maintained by health care personnel including doctors and nurses, then man-made things can be maintained by engineers.

As just an engineer, what could I do for society on earth? What could I do, as an educator, for young people? One could certainly create novel things to attract people's attention as in the Expos in the past. Inventors could feel excited about and satisfied with them. Behind that, however, people are involved in wasteful volume consumption, which is threatening the globe. It is now necessary to undergo a paradigm shift from robotics that can just satisfy the mega-corporations' needs for high-volume production for higher profits to another robotics as a new methodology for mankind to survive.

Even after two years of agonizing over such issues, I have not yet reached a solid conclusion. Still, there is a challenge I am now trying to address. It is modular robots.

* Professor at Ritsumeikan University

2. Modular Robot Project

Based on the social and natural environments we are in, needs will rapidly increase for civil engineering and construction, transportation, and facility maintenance operations in basically non-accessible environments, such as in agriculture, forestry and fishery, infrastructure maintenance, and disaster recovery. In response to these various novel needs, not only high-performance robot equipment but also total robot solutions that can reduce the operators' burden and costs are needed.

One of the potential concepts for such solutions is modular robots. Multiple single-function robots working independently can be combined with each other to become a robot assembly that can flexibly perform various tasks. These modular robots offer many operational benefits, including structure selection and allocation with the right robots in the right place, maneuverability and portability, and easy manufacturing and maintenance. Reconfigurable robots and self-organized robots already exist in the academic area. These can be defined as robot systems to achieve a specific purpose while adapting their own shape to indefinite circumstances. Many papers in the past have showed examples of concepts or simulations where a number of objects of similar morphology are combined to become an assembly forming a specific structure. However, most of these papers relied on computer graphics (CG) based studies mainly using planning algorithms. Actual machine-based studies of this kind mainly covered group displacement robots. Attempts to accomplish heavy duty tasks that are generally assumed to be done by outdoor robots have seldom been made.

Our challenge is to integrate modular robots with hydraulics. Specifically, we are thinking of maximizing the robustness and high output specific to hydraulics as well as the protean power collection and distribution capability of hydraulic circuits and piping. The former was introduced in the Technology Introduction article titled *Development of a Hydraulic Module Robot* included in KYB Technical Review No.61 in 2020. The latter concept was presented at the International Conference on Robotics and Automation (ICRA) of Institute of Electrical and Electronics Engineers (IEEE) in 2022.

For comparison purposes, let me take conventional

hydraulic machinery. For example, hydraulic excavators have arms similar in shape to those of industrial manipulators. They can show great activity for disaster recovery as powerful and reliable robots, although they are seldom used as autonomous machinery. The front-end part is highly modularized to accept a variety of attachments. For hydraulic excavators, hydraulic equipment manufacturers provide various actuators as discrete components, including cylinders, valves, and pumps. Still, it is difficult to modularize these actuators because of the design of hydraulic excavators wherein their drives are located at the root of the machinery.

Industrial actuators integrated with drive sources represented by electro-hydraulic actuators (EHAs) have recently become commercially available. Using this type of actuator will realize robot modules integrated with a hydraulic source, although the power supply challenge remains. However, such simple integration would inevitably result in robots with too heavy front ends, leading to an overall deterioration in performance. What impedes modularization is essentially weight. Could it be possible to realize a modular robot that can be manually carried and assembled by people and is able to lift loads at least equivalent to its own weight, although it could not be so modularized that it could easily be assembled by hand like hobby robots? If attachment and detachment of modular parts can be automated, the robot can also assemble itself without human intervention.

This research project considers the potential of hydraulics in several areas:

A) The use of small pumps will allow robots to deliver high output with small motors although the motor speed is low.
B) For light loads, external pumps can be used to move robots with agility.
C) Possible to manufacture shock-resistant, weatherproof robots at low cost.
D) Robot power can be monitored and controlled by means of pressure.
E) Pressure boosting and merging will allow multiple shafts to interchange power.
F) Parts attachment and detachment can be achieved with hydraulics.

Based on these ideas, research challenges were set up and a research plan developed.

Certainly, robots that are mechanically merged and assembled are substantially inferior in performance to optimally-designed integrated robots. Is this always true? A question to be posed is, based on the operational needs mentioned at the outset, "what are the conditions that give hydraulic modular robots advantages to conventional integrated robots?" Note that conventional robots include pure electric robots. It is important to specifically verify several hypotheses.

3. Epilog

Under the big slogan of the paradigm shift from tangible to intangible goods, people's interest in tangible goods has diminished. Equipment mechanisms are hidden like a black box and treated as second-rate things to be consumed in an instant, like something on a smartphone screen. It is certainly good to get things done easily, but how many engineers who can understand and interact with mechanisms of tangible products would survive in Japan if the tendency of people to move away from tangible goods is going to progress in this pace? The same thing can be applied to artificial intelligence (AI). Being indifferent to technology can be considered as a kind of abandonment of thinking. It is very dangerous to leave advanced robot technology to just a few people.

Renovation and similar concepts (including sustainable design) will increasingly affect how people face nature or artifacts. Concepts of these kinds always involve inconspicuous and rough-and-ready impressions, rather than brave, stereotype cutting-edge images as seen in great discoveries of novel materials or big inventions regarding their application. Moreover, they are very hard work requiring people to be patient and cannot be achieved without deep understanding of tangible goods and technology. I heard that, under this situation, more and more young people have started to feel something strange about mass production and volume consumption. They tend to love traditional or old things and are trying to put their own ideas into them to produce additional value. This is definitely good news.

To cause renovation to sublimate into science, new insights and methodologies are needed. Hydraulic modular robots could be considered as products of renovation of conventional hydraulic machinery. From the new perspective of modular robots, we can say we are trying to take lessons from history or hydraulic technology that can be considered well established. While conventional robotics might play the passive role of just responding to the industrial world's needs (mass production), new robotics should be "technology for all" with which people can voluntarily and boldly address difficult issues in the Anthropocene era. Thinking patiently, we want to repeatedly make and verify assumptions for as long as time permits.

Finally, I would like to take this opportunity to thank KYB Corporation for their support for research and education at Ritsumeikan University. While many people are anxious about the sharply worsening issues of global warming, the COVID-19 pandemic, and food and resource risks, I hope that all engineers from KYB will continue to proudly support society more and more and work toward Monozukuri that can save the earth.

Technology Introduction

Making Plating Thickness Constant by Simulation

MIZUNO Yuuki, TERADO Ayuko

1 Introduction

Recent years have seen the promotion of digital technologies including artificial intelligence (AI) and Internet of Things (IoT) in virtually all fields. Even techniques that have long been conveyed as craftmanship are becoming subject to standardization with digital technologies.

KYB Corporation frequently applies hard chrome plating to sliding parts of shock absorber piston rods and other components. This plating requires masking jigs (hereinafter "jigs") Note 1) because of its characteristics. Conventional jig design relies on work learned only through actual experience (so-called knack or intuition) of operators. It is difficult to achieve constant deposition of plating (hereinafter "film thickness"). Since jig fabrication and plating prototyping are needed for each try, many man-hours are spent to discuss and determine the form of jigs Note 2) (Fig. 1). With this background, KYB has developed a jig design methodology requiring no knack or intuition by utilizing simulation software. This paper introduces a case study of our efforts to achieve constant plating thickness of industrial hydraulic equipment products by means of simulation.

Note 1) Masking jigs used to prevent plating or limit the film thickness

Note 2) Three to four tries were needed before completion: 2 weeks/try

(according to interviews with operators)

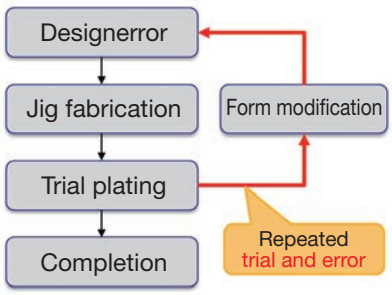

Fig. 1 Conventional jig design flow

2 Characteristics of Electroplating

This chapter describes the major characteristics of electroplating including hard chrome plating. For electroplating, the film thickness is generally proportional to the quantity of electricity (current × time) (Faraday's 1st law).

When applying plating to workpieces, the current is likely to concentrate at the edges of them, resulting in thicker films (Fig. 2). This phenomenon can be prevented by the use of shorter electrodes. In facilities where workpieces of different lengths are plated, however, just changing the length of the electrode would not be enough. Then, jigs can be installed at the edges of a workpiece to suppress the concentration of the current at the edges, curbing the increase in plating thickness.

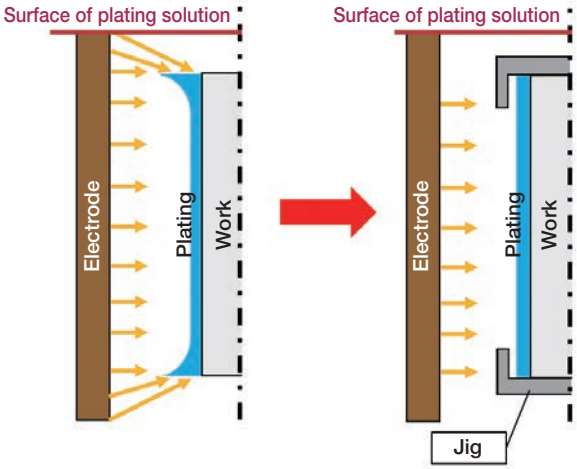

Fig. 2 Illustration of effects of jigs

3 Preliminary Test on Stepped Work

Before redesigning the jig through simulation, a preliminary test was conducted using a stepped workpiece. Fig. 3 shows the front view of the preliminary test equipment. The workpiece and electrodes are vertically inserted into the plating bath. In total four electrodes are installed around the workpiece. This stepped workpiece consists of thick and narrow sections: the former has a diameter of ø22 and the latter ø10. All of these sections, regardless of the diameter, are 100 mm long. The test conditions are shown in Table 1. As mentioned in the previous chapter,

the edges or corners of the workpiece are likely to have higher current density which builds thicker films. The test was carried out to verify whether this phenomenon can be reproduced in simulation.

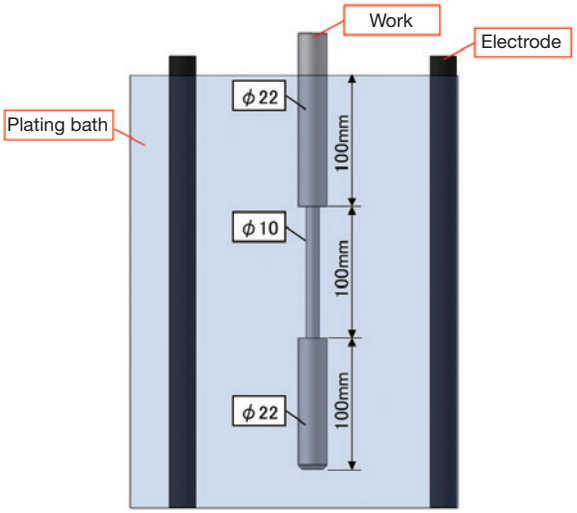

Fig. 3 Sketch of preliminary test equipment

Table 1 Plating conditions for preliminary test

Item	Settings
Plating bath	Sargent bath
Plating solution temperature	50°C
Plating area	1.7 dm^2
Current density	40 A/dm^2
Current setting	70 A
Plating time	30 min.

The simulation software used for this research is intended to be used for analysis of current density (A/dm^2). Since analysis results cannot be directly compared with film thickness measurements, the analysis results (A/dm^2) have been converted into the film thickness (μm) using Equation (hereinafter "Eq.") (1):

$$\text{Film thickness } \mu m = \text{Deposition speed } \mu m/min \cdot A \cdot dm^{-2} \times \text{Current density } A/dm^2 \times \text{Plating time min} \times \text{Current efficiency} \quad (1)$$

A contour diagram of the analysis results is shown in Fig. 4. For convenience, the top section of ø22 is called A, the middle section of ø10 called B, and the bottom section of ø22 called C. The edges of sections A and C as well as the central part of section B have a higher current density, while the edges of section B have a lower current density.

Comparison between the analysis results and the measurements are shown in Figs. 5 to 7. For the purpose of this paper, the "film thickness" (vertical axis) in the Figures indicates individual measurements that have been divided by the mean value of the film thickness of the flat parts (A: 10 mm to 60 mm, B: 130 mm to 170 mm, C: 230 mm to 270 mm) of the workpiece and then made dimensionless.

The trends of film thickness distribution of sections A, B and C obtained through simulation almost match those obtained through actual measurement. Therefore, the use

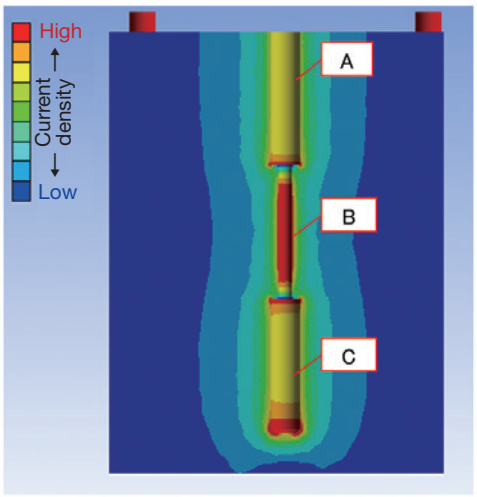

Fig. 4 Analysis results (current density distribution)

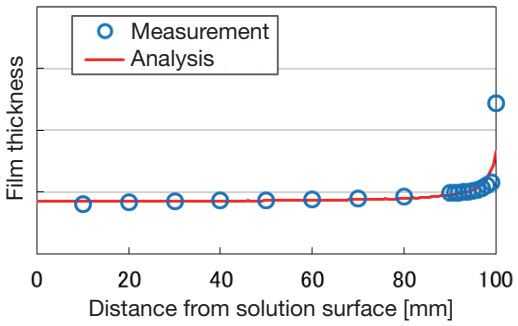

Fig. 5 Comparison in section A

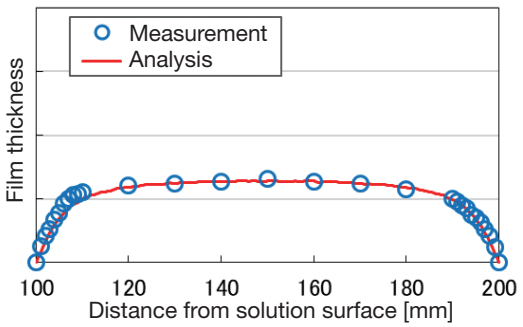

Fig. 6 Comparison in section B

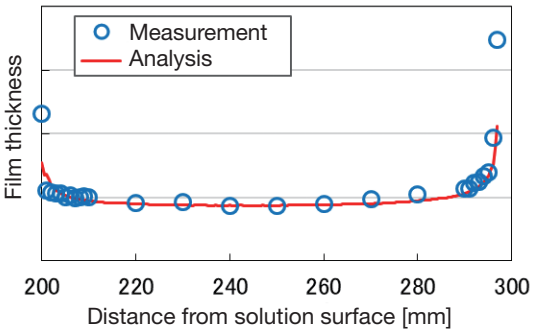

Fig. 7 Comparison in section C

of the simulation model and conditions developed for the research can be used to obtain a film thickness distribution similar to the actual phenomenon.

4 Making Film Thickness Constant

Since the simulation model was validated through the preliminary test, its utilization in mass production equipment was tried.

4.1 Target Product

The piston rods for forklift cylinders were selected as the target product (Fig. 8).

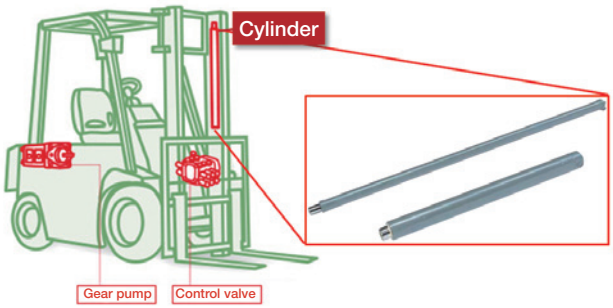

Fig. 8 Target product

4.2 Conventional Jig

Fig. 9 shows measurements of plating thickness obtained with the conventional jig (Photo 1). An electromagnetic plating thickness gauge was used to measure the film thickness of workpieces longitudinally along a straight line. The Figure includes a sketch of the workpiece installed with the jig.

The jig design was based on operators' knack and intuition, resulting in uneven film thicknesses. In particular, the masked portion had a substantially lower film thickness. To compensate for the film thickness in this portion, thicker plating was made overall. This led to longer plating time and consumed extra electricity and chemicals.

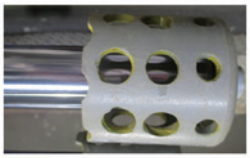

Photo 1 Conventional jig

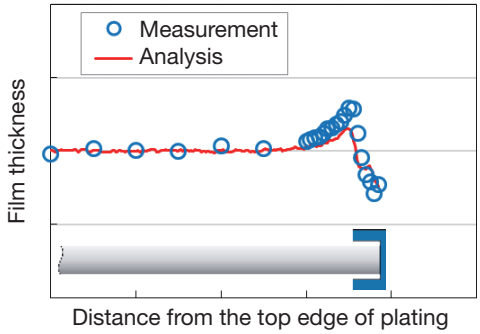

Fig. 9 Comparison between measurement and simulation (conventional jig)

While the central part of the rod has a constant film thickness, the edges of the rod have uneven film thicknesses due to the concentrated current and the shielding effect of the jig. Through comparison with the simulation results, it was verified that the tendency of the film thickness distribution was successfully reproduced.

4.3 Redesigning the Jig

To make the current density distribution indicated by the analysis results more uniform, we tried to find an optimal form of the jig by repeatedly changing and analyzing the aspect ratio, hole diameter and the number of holes of the jig model (Fig. 10). This redesigning was carefully conducted because the current density distribution greatly varies with the jig form (Fig. 11). The authors

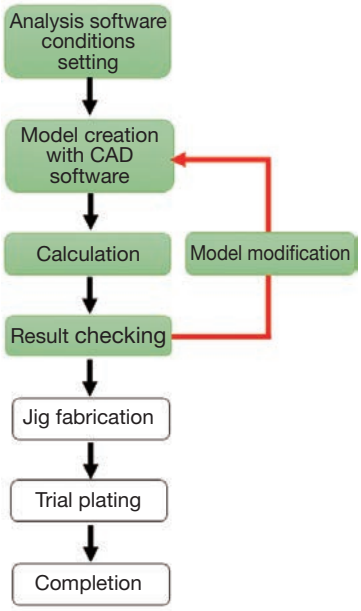

Fig. 10 Jig design flow using simulation software

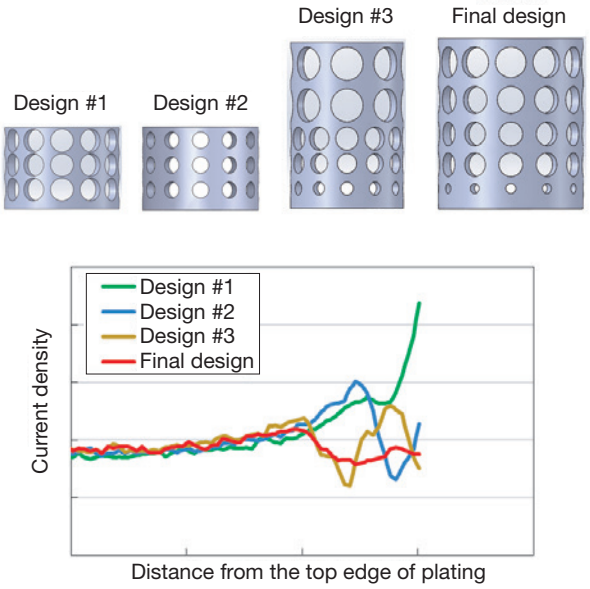

Fig. 11 Analysis results of various jig model versions

had no previous experience of jig form design. After about two weeks of redesigning work, the "final design" included in Fig. 11 was obtained through repetitive modification of the jig model.

As indicated by the workflow in Fig. 10, the simulation cycle was effectively used to successfully fabricate the jig and verify the plating with a single try.

4.4 Verifying the Effect

The jig prototype obtained through the jig fabrication and trial plating processes was compared with the conventional jig. For the purpose of this paper, the prototype is called the "improved jig" (Photo 2). Fig. 12 shows film thickness measurements with the conventional and improved jigs. The film thickness variation {(Maximum film thickness - Minimum film thickness) / Mean film thickness} of the conventional jig was 57% of the mean film thickness. In contrast, the film thickness distribution of the improved jig was as low as 11% of the mean value.

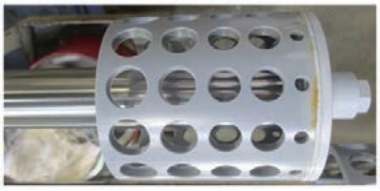

Photo 2 Improved jig

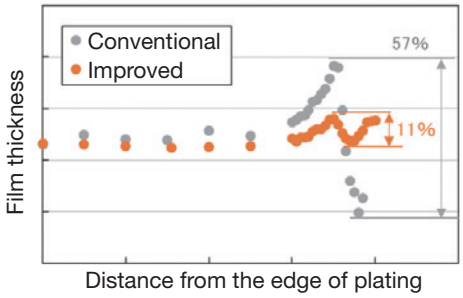

Fig. 12 Comparison of film thickness measurements

5 Further Efforts for Even Higher Efficiency

The company's traditional jig improvement relied on operators' knack and intuition and the redesigning required about six weeks. For the authors' jig improvement through simulation, the redesigning time was reduced to two weeks. However, the model improvement through simulation involved repetitive trial and error and could not completely exclude the dependence on operators' knack and intuition. The reduction of improvement time remains a big challenge even after the introduction of simulation.

Then, we tried to reduce the redesigning time and eliminate the dependence on knack and intuition by introducing an optimization software product [Note 3)] to allow the model modification and calculation processes to be done automatically (Fig. 13).

Note 3) Software used: Simcenter HEEDS®

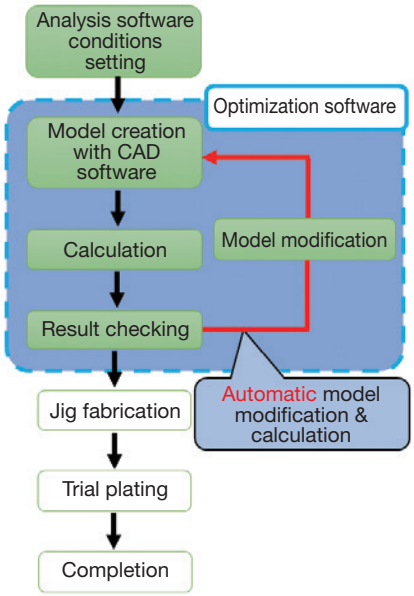

Fig. 13 Jig design flow using optimization software

5.1 Conditions Setting

For the purpose of redesigning the jig, the five parameters listed in Table 2 were selected for conditions setting in the optimization software. 100 combinations of parameter settings were subjected to calculation by the software to determine the jig form with the smallest variation in film thickness. Fig. 14 shows what the parameters indicate in the actual jig.

Table 2 Parameter settings for optimization software

Parameter settings	
Outside diameter	ø47-85 mm
Height	5-130 mm
Hole diameter	ø1-30 mm
Number of longitudinally aligned holes	2-10
Number of circumferentially aligned holes	4-20

100 combinations of parameter settings were analyzed.

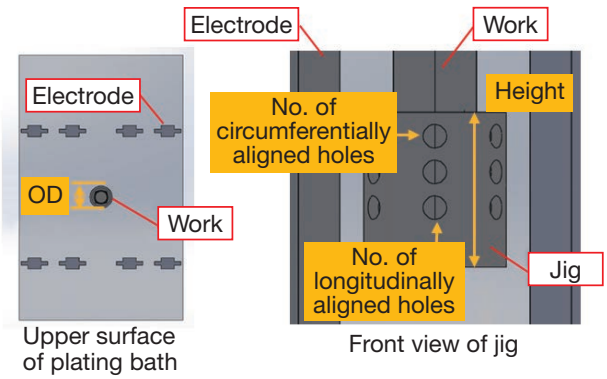

Fig. 14 Locations of parameters

5.2 Film Thickness Measurements

The model obtained through calculation using the optimization software was used to fabricate a jig (Photo 3). This jig was trial plated and then subjected to measurement of film thickness.

As shown in Fig. 15, the film thickness variations were reduced to about 1/3 (19%) of those of the conventional jig, although this result was inferior to that of the improved model (11%) obtained only through the simulation software. Furthermore, the redesigning time was reduced to as little as eight hours, which is about 1/10 of the time spent for the improved jig (i.e., two weeks: equivalent to 80 working hours). Thus, "anyone" can now "easily" design a jig in a "short time" just by entering the five parameters.

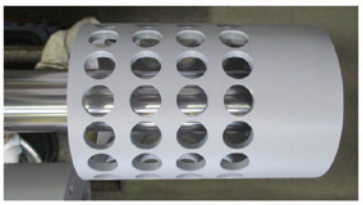

Photo 3 Improved jig Ver.2

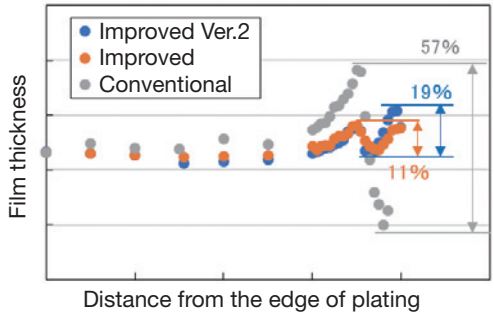

Fig. 15 Comparison of film thickness measurements #2

6 Future Prospects

Additional expected benefits from this effort include lower processing costs (for electricity and chemicals) and lower CO_2 emissions due to shorter plating time.

Plating should be applied to applicable products to ensure that the thinnest part of the plating film meets the film thickness requirements. However, conventional plating has been applied based on the film thickness at the edges, which is lower as shown in Fig. 16. Plating in this way will provide an excessive film thickness on the flat part that is away from the edges of the plated work. Then, the improved jig can be used to ensure work has a higher film thickness at the edges than on the flat part, thereby enabling the excess in film thickness to be eliminated (see the shaded zone in Fig. 16). The plating time can also be reduced by an amount corresponding to the film thickness reduction, leading to lower processing cost and lower CO_2 emissions.

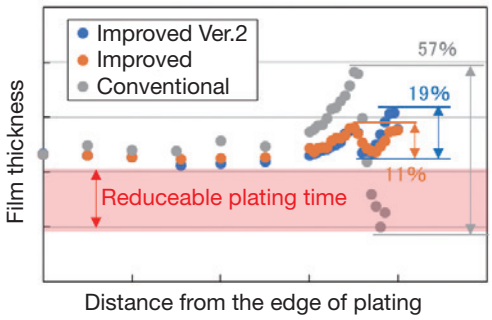

Fig. 16 Expected benefits

7 In Closing

It was verified that the simulation is very effective for achieving constant plating films and higher productivity. In addition, the utilization of the optimization software was shown to enable jig redesigning that does not depend on knack and intuition and a substantial reduction in redesigning time.

The simulation can also be expected to be utilized to find causes of inappropriate film thickness or even for discussion of the specifications for new plating lines (such as throughput). KYB operates a variety of working processes including heat treatment and cutting as well as plating. It is desirable to effectively apply the simulation methodology not only to plating but also to various other working processes.

Finally, we would like to take this opportunity to sincerely thank all those concerned inside and outside KYB who have extended cooperation to this development.

Author

MIZUNO Yuuki

Joined the company in 2019.
R&D Sect. No.1, Production Technology R&D Center, Engineering Div.
Engaged in development of surface treatment technology

TERADO Ayuko

Joined the company in 2012.
R&D Sect. No.1, Production Technology R&D Center, Engineering Div.
Engaged in development of surface treatment technology

Technology Explanation

Control Technologies for In-Vehicle Electric Actuators

MATSUMOTO Daisuke, ENOMOTO Daisuke, KENJO Kazunori, FUKUSHI Natsuru

Abstract

KYB develops and manufactures various in-vehicle actuators including electric power steering (EPS). The control specifications of the actuator differ depending on the function, but it is a common issue to achieve a system that operates stably and satisfies the required functions and performance. In addition, when controlling the actuator, the control system may become unstable depending on the design of the control compensator, so it is necessary to design the compensator after grasping the characteristics of the actuator to be controlled.

In this report, we explain the compensator design method for the steering assist control of EPS for all terrain vehicles and utility task vehicles and for steering angle control with an eye toward future application in automatic steering, as well as the implementation method of this design method. This report also describes the future outlook.

1 Introduction

Compared with electric power steering (EPS) for passenger vehicles, EPS for all-terrain and utility task vehicles, particularly for off-road vehicles, is required to deliver more highly responsive steering assist and kickback control performance. To satisfy these performance requirements, it is a precondition that the EPS hardware (including the motor described later and its driving circuit, gear assembly, etc.) has been properly designed. In addition, it is necessary to maximize the hardware capabilities by using software (i.e., with a proper control methodology). Specifically, the open-loop gain of the control system (a gain of the loop transfer function) must be set to a level as large as possible within the frequency ranges in which the steering assist and kickback control performance are required. However, care must be exercised in setting the open-loop gain because just using a high open-loop gain would reduce the gain and phase margins (hereinafter "stability margin"), resulting in an unstable control system in some cases. As an approach to ensure a stability margin while using a high open-loop gain (hereinafter "stabilization"), a phase compensator Note 1) has been used. For stabilization using this approach, the phase compensator is designed with a focus on the gain and phase information of the frequency characteristics of the loop transfer function of the control system (called a "non-parametric model"). It is relatively easy to implement a phase compensator, but designers need to adjust design parameters through trial and error while carefully observing the frequency characteristics. This means that such designers need to have a certain level of experience and knack. As described later, the compensator is assumed to be redesigned in phases during the development stage. For higher efficiency in development, it is desirable to automate the compensator development processes, including from design to implementation, to some extent. However, design tool automation can hardly be achieved by conventional approaches.

Note 1) The compensator in a control system is a computing unit intended to generate control input to impart desirable characteristics to the system. A phase compensator is designed with a focus on the gain and phase of the loop transfer function of the control system.

On the other hand, robust control theory, typified by the H_∞ control theory, involves approaches that use the transfer function and state equation of the controlled object (called a "parametric model") to design the compensator through inverse operation from the desirable characteristics (target tracking and disturbance response) of the control system. In these approaches, the controlled object, the characteristics of the control system, and disturbances are represented by parametric models and the related various equations are solved to determine the compensator. This means that design tools can relatively easily be automated, delivering the benefit that compensators can be designed more efficiently. These design approaches may be effective to catch up with the rapid development specific to the all-terrain and utility task vehicles market.

In general, compensators designed based on robust control theory tend to be more complicated (with higher degree) than phase compensators. However, in-vehicle microprocessors mounted with floating point units (FPUs) have been generally introduced in recent years to allow

implementation of compensators of relatively high degree.

This report explains how to design steering assist and steering angle control compensators for EPS based on the parametrization of stabilizing compensators [3], which is one of the basic theories of robust control.

2 EPS Systems

2.1 Components of EPS System

Fig. 1 shows the components of the EPS for all-terrain and utility task vehicles.

The electromechanical brushless motor shown in the Figure (hereinafter "the power pack") is a brushless motor integrated with a controller (hereinafter "the motor") as the name implies. This component performs computations for all controls including steering assist control.

The torque angle sensor (TAS) is another component that detects the torque and angle of the steering wheel operated by the driver. The steering assist control uses torque values detected by the TAS as described later. The steering angle control uses angle values detected by the TAS to set the origin of the steering angle that is calculated from the motor rotation angle.

The gear assembly has a mechanism by which the torque generated by the motor is amplified by a worm reducer and this rotary motion is converted into a linear motion by a rack and pinion device. This component transfers the steering torque produced by the driver and the steering assist torque generated by the motor to the vehicle's wheels as a cornering force.

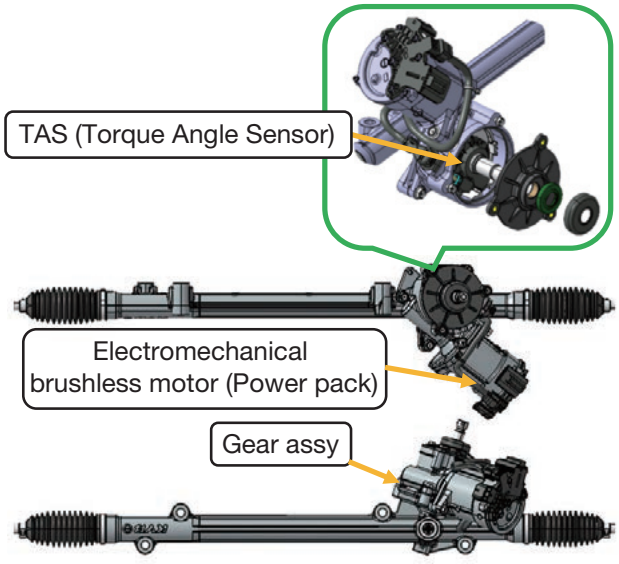

Fig. 1 EPS components for all-terrain and utility task vehicles

2.2 Block Diagram of EPS System

Fig. 2 is a block diagram of the EPS system.

The controller has three major functions; ① A monitoring function to detect any abnormality of the CPU, driving circuit and sensors, and perform fail-safe processing, ② A communication function to communicate with the vehicle and other sub systems via a CAN network, and ③ Control functions including motor vector control, steering assist control, and steering angle control.

With a focus on the steering assist and steering angle controls, the next chapter describes how to design compensators for these controls.

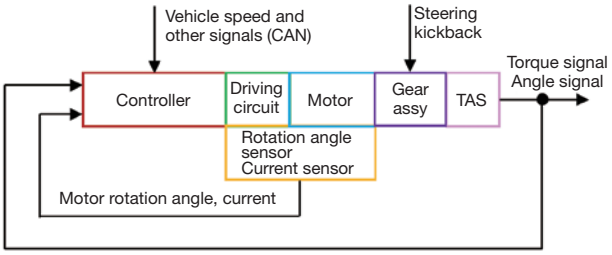

Fig. 2 Block diagram of EPS system

3 Overview of Compensator Design

3.1 Components of Control System

Fig. 3 shows an overview of the control system (the controlled object + compensator) with a focus on the steering assist control or steering angle control.

The control input to this control system is from motor current commands. The control output from the system is steering angle or torque values from the TAS (the steering angle is calculated from the motor rotation angle). The load torque is attributable to the driver's steering and kickback transferred to the motor via the gear assembly and the friction torque of the gear assembly.

In the Figure, the area enclosed by the red broken line represents the controlled object, which is a mixed system of hardware and software. The former includes the motor, the driving circuit, the controller, and the gear assembly, and the latter is for motor vector control and steering angle computation.

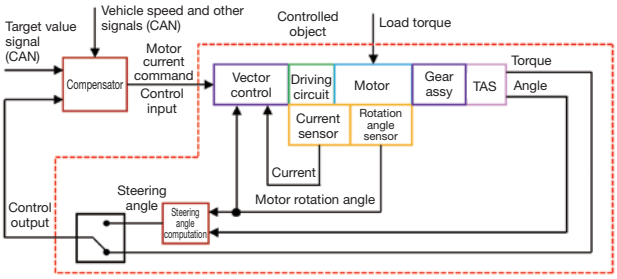

Fig. 3 Overview of control system

3.2 Compensator Design Policy

Within the controlled object shown in Fig. 3 in the previous section, the hardware including the driving circuit, motor, and gear assembly behaves electrically or mechanically in real time. With these physical phenomena, the hardware constitutes a continuous time system. On the other hand, the software is a discrete time system [Note 2] because vector control and steering angle computation are

performed by digital computers. Therefore, the actual controlled object is a mixed system of continuous and discrete time systems. The control input to and output from the controlled object are updated or sampled at each of their own control frequencies. That is, the controlled object ranging from the control input to the control output can be represented by a discrete time model Note 3). The compensator can also be represented by a discrete time model because its computation is performed by digital computers.

Note 2) A system whose behavior is defined with discrete time (hereinafter "sampling time").

Note 3) A discrete time model is a difference equation or transfer function representation of the behavior of the controlled object under the control of a digital computer at a sampling time or the behavior of a discrete time system.

Conventionally, the set of the controlled object and compensator has been considered as a continuous time system. In this approach, the compensator is designed according to continuous time and then discretized using, for example, a bilinear expression before implementation. This approach has the problem that design stability cannot be ensured in actual systems. One major factor is that a compensator that has been discretized with a bilinear expression, for instance, cannot necessarily become a stabilizing compensator for the discrete time system (i.e., the stability margin for the discrete time system cannot be guaranteed) (Challenge ①). Another major factor relates to modeling error of the controlled object (discrepancy between the model and the actual system). The system cannot be stable if the designed compensator was not a stabilizing compensator for the actual system in the first place (Challenge ②). To address Challenge ①, it is useful to represent the controlled object as a discrete time model and design the compensator according to the discrete time system. For Challenge ②, it is effective to use the frequency response method or the method of identification [4] using maximum-length sequence signals to determine a model for designing the compensator (hereinafter a "compensator design model"). Then, we have decided to introduce the approach of representing the controlled object in a discrete time model and designing the compensator in a discrete time system. We also identify the system to be controlled upon completion of the hardware fabrication and design the compensator using the identified compensator design model. We use δ (delta) operator [5] as a discrete time operator representing the controlled object and compensator model. The δ operator can be expressed as $\delta = (z - 1)/T_c$ (where z is the z operator and T_c is control frequency). A major advantage of using the δ operator is that relatively high accuracy can be obtained with compensator computation with a low number of bits. For more information, see References [4), 5)].

3.3 Block Diagram of Control System

The controlled object included in the control system shown in Fig. 3 can be approximately represented by a block diagram as shown in Fig. 4:

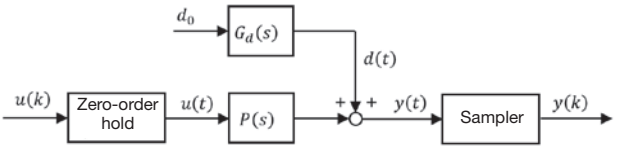

Fig. 4 Block diagram of controlled object (continuous time system)

$P(s)$ in Fig. 4 is the continuous time model (transfer function) of the controlled object. k is an integer not less than 0 (zero) used to indicate the sampling time [$t_s(k) = kT_c$ ($k = 0, 1, ...$)]. $u(k)$ is the output from the compensator, namely, control input (motor current command). $u(t)$ is $u(k)$ held every "time" $t_s(k)$. $y(k)$ is the control output that is $y(t)$ sampled every "time" $t_s(k)$. Control output $y(k)$ will be a TAS torque signal for steering assist control or a steering angle for steering angle control. $d(t)$ is the disturbance attributable to the load torque shown in Fig. 3 and the rotation of the steering wheel operated by the driver. d_0 is a constant. $G_d(s)$ is the transfer function representing a disturbance generator. Note that $u(t)$ and $u(k)$ are signals that are different from $y(t)$ and $y(k)$ signals, but for convenience these are not differentiated by symbols.

The block diagram of Fig. 4 may be represented by a discrete time system as shown in Fig. 5. $P(\delta)$ and $G_d(\delta)$ are transfer functions (discrete time models) obtained by zero-order holding and discretization $P(s)$ and G_d (s) with a sampler, respectively. Note that $P(s)$ and P(δ) are transfer functions that are different from G_d (s) and $G_d(\delta)$ transfer functions, but for convenience these are also not differentiated by symbols.

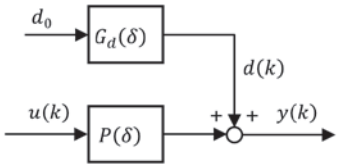

Fig. 5 Block diagram of controlled object (discrete time system)

Thus, the control system in Fig. 3 can be represented using the transfer function model $P(\delta)$ of the controlled object and the transfer function model $C(\delta)$ of the compensator as shown in Fig. 6. In Fig. 6, $r(k)$ is the target steering angle signal. r_0 is a constant. $G_r(\delta)$ is the transfer function representing the target value signal generator. This report describes how to design a compensator $C(\delta)$ for the control system in Fig. 6. Note that $C(\delta)$ is assumed to be a two-degree-of-freedom controller as follows:

$$C(\delta) = [C_r(\delta) \quad C_y(\delta)] \tag{1-1}$$

$$u(k) = C_r(\delta)r(k) - C_y(\delta)y(k) \tag{1-2}$$

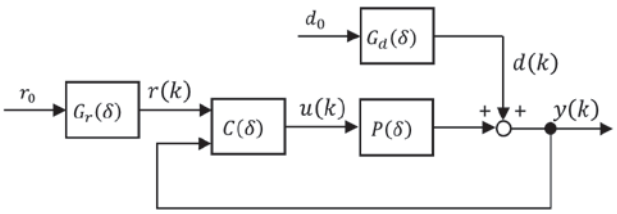

Fig. 6 Block diagram of control system

3.4 Compensator Design Flow

Fig. 7 shows the compensator design flow as a V-shaped process diagram. This section describes what to do in each of the design processes (the flow to the left in Fig. 7).

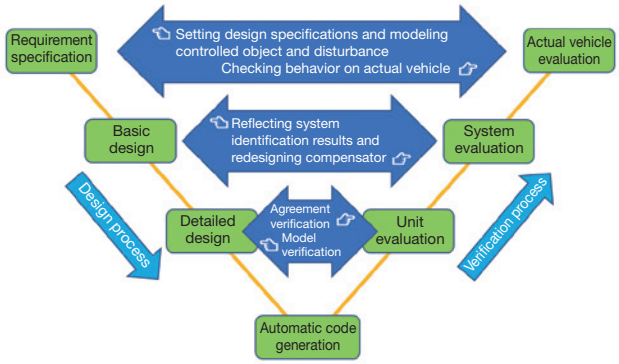

Fig. 7 V-shaped process of compensator design

3.4.1 Requirement Specification

The following describes what to do in the Requirement Specification stage.

(1) Setting design specifications

For steering assist control, an assist map where motor current commands are mapped against TAS torque signals is used to set the assist torque. A higher assist torque means a larger open-loop gain. A major requirement for the design specifications is that the required assist torque can be generated stably (i.e., without issuing harmful vibration). In other words, the control system will remain stable even with the maximum assumed open-loop gain.

For steering angle control, the steering angle will follow the target steering angle signal $r(k)$ in Fig. 6. Major design specifications include, for example, delay time, rise time, setting time, overshoot, and steady-state deviation to $r(k)$ that may change stepwise or in ramp rate.

(2) Modeling controlled object and disturbances

Controlled object models can roughly be divided into two types. One is a high-precision simulation model [6] that can estimate in relative detail the behavior of the actual system (hereinafter "the simulation model"). The other is a simplified model for designing compensators (the aforementioned compensator design model). A compensator design model can be derived from a differential equation that has linearized and simplified the controlled object. A compensator design model can also be derived through identification of a system using the simulation model or actual machine. The identification of systems using an actual machine will be described later. The simulation model can be created and implemented mainly by using tools such as MATLAB®/Simulink® and SimulationX®.

The disturbances that may be applied to the controlled object include; ① Rotation of the steering wheel operated by the driver (for steering assist control), ② Load torque due to kickback, and ③ Friction torque of the gear assembly. For steering assist control, these disturbances can be represented by a transfer function model with an assumption of steering frequency as described later. For steering angle control in turn, the disturbances should be represented by a step or ramp function model based on the assumption that, with the driver's hands off the steering wheel, the steering angle can follow the steering angle command without steady-state deviation under disturbances ② and ③.

3.4.2 Basic Design

In the basic design stage, a compensator is designed using the compensator design model and the assumed disturbance model. The compensator can be expressed by a transfer function model $C(\delta)$ in this stage. The simulation model and the designed compensator are used to carry out simulation and verify the adequateness of the compensator during this stage. The compensator design will be described in detail in Chapter 4.

3.4.3 Detailed Design

In the detailed design stage, the compensator designed in the basic design stage is developed into an implementation model to be contained in the controller as software. This stage should verify that the compensator $C(\delta)$ derived in the basic design stage is equivalent to the implementation model (i.e., identical inputs will produce the same output).

3.4.4 Automatic Code Generation

Embedded Coder® is used to automatically generate codes from the implementation model.

4 Compensator Design

This chapter describes the details of the basic design of compensators for steering assist control and steering angle control. The compensator design for steering assist control is different from that for steering angle control in control output, design specifications, and disturbances. The two compensators can be applied with the same design approach.

4.1 Basic Design of Steering Assist Control Compensator

4.1.1 Deriving a Compensator Design Model

An EPS model is shown in Fig. 8:

The EPS shown in Fig. 8 is a single-pinion type. This model can also be applied to double-pinion or column

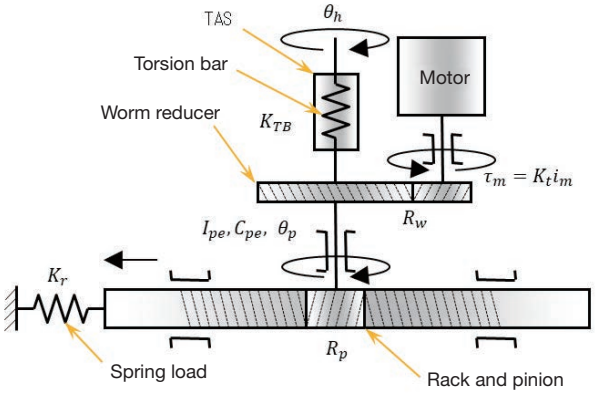

Fig. 8 EPS model

EPS. The symbols used in the figure indicate the following:

θ_h : Rotation angle of steering wheel [rad]
θ_p : Rotation angle of pinion [rad]
i_m : Motor current [A], τ_m: Motor torque [N·m]
K_t : Motor torque constant [N·m/A]
K_{TB} : Spring constant of torsion bar [N·m/rad]
R_w : Reduction ratio of worm reducer
I_{pe} : Equivalent inertia moment of pinion shaft [kg·m^2]
C_{pe} : Equivalent viscous resistance coefficient of pinion shaft [N·m/(rad/s)]
R_p : Specific stroke of rack and pinion [m/rad]
K_r : Spring constant of rack load [N·m/rad]

The TAS torque signal can be expressed by the equation below:

$$\tau_s = K_{TB}(\theta_h - \theta_p) \tag{2-1}$$

Assuming that i_m is equal to u (the actual current completely follows the motor current command) and that all the parts except the torsion bar are rigid bodies, the rotary motion of the pinion can be expressed by the differential equation below:

$$I_{pe}\ddot{\theta}_p + C_{pe}\dot{\theta}_p = R_w K_t i_m + K_{TB}(\theta_h - \theta_p) - K_r R_p^2 \theta_p \tag{2-2}$$

where

$$i_m = u$$

From Eqs. (2-1) and (2-2), the following state and output equations can be obtained:

$$\dot{x} = A_P x + B_P u + E_P \theta_h \tag{2-3}$$

$$y = C_P x + F_P \theta_h \tag{2-4}$$

where

$x = [\theta_p \quad \dot{\theta}_p]^T$: State variable, $y = -\tau_s$: Control output
u: Control input (motor current command)

$$A_P = \begin{bmatrix} 0 & 1 \\ -K_{pe}/I_{pe} & -C_{pe}/I_{pe} \end{bmatrix},\ K_{pe} = K_{TB} + K_r R_p^2$$

$$B_P = \begin{bmatrix} 0 \\ R_w K_t / I_{pe} \end{bmatrix},\ C_P = [K_{TB} \quad 0]$$

$$E_P = \begin{bmatrix} 0 \\ K_{TB}/I_{pe} \end{bmatrix},\ F_P = -K_{TB}$$

In Eqs. (2-3) and (2-4), if θ_h is 0, the state and output equations for the discrete time model can be expressed by the equations below:

$$\delta x(k) = A_{P\delta} x(k) + B_{P\delta} u(k) \tag{3-1}$$

$$y(k) = C_{P\delta} x(k) \tag{3-2}$$

where

$A_{P\delta} = (A_{Pz} - I_2)/T_c$, I_2: 2 × 2 unit matrix
$B_{P\delta} = B_{Pz}/T_c$, $C_{P\delta} = C_{Pz} = C_P$
$A_{Pz} = e^{A_P T_c}$, $B_{Pz} = \int_0^{T_c} e^{A_P T_c} d\tau\, B_P$

A_{Pz}, B_{Pz} and C_{Pz} are a system/control matrix where Eq. (2-3) or (2-4) is discretized by the z operator each. These can be determined using the discretization method "zoh" using the MATLAB® function "c2dm". Eqs. (3-1) and (3-2) are called step invariant models [5] of Eqs. (2-3) and (2-4). When Eqs. (3-1) and (3-2) are selected for the compensator design model, the transfer function $P(\delta)$ in Figs. 5 and 6 can be expressed by the equation below:

$$P(\delta) = C_{P\delta}(\delta I_2 - A_{P\delta})^{-1} B_{P\delta} = \frac{n_P(\delta)}{d_P(\delta)} = \frac{n_{P1}\delta + n_{P0}}{\delta^2 + d_{P1}\delta + d_{P0}} \tag{3-3}$$

In the initial development stage where the detailed design of hardware has not been completed, Eqs. (3-1) to (3-3) should be used as compensator design models to design compensators. However, these models may need to be revised when specific hardware specifications are made available or when the hardware fabrication has been completed. With consideration given to these cases, the degree of the compensator design models (degree of the denominator polynomial $d_p(\delta)$) is assumed to be 'n' in the following discussion. Then, the transfer function $P(\delta)$ is expressed by the equation below:

$$P(\delta) = \frac{n_P(\delta)}{d_P(\delta)} = \frac{n_{Pn-1}\delta^{n-1} + \cdots + n_{P1}\delta + n_{P0}}{\delta^n + d_{Pn-1}\delta^{n-1} + \cdots + d_{P1}\delta + d_{P0}} \tag{3-4}$$

4.1.2 Setting Disturbance Models

This section discusses disturbance models of degree l that can be expressed by the equations below:

$$d = G_d(s) d_0 \tag{4-1}$$

$$G_d(s) = \frac{n_d(s)}{d_d(s)} = \frac{n_{dl-1}s^{l-1} + \cdots n_{d1}s + n_{d0}}{s^l + d_{dl-1}s^{l-1} + \cdots d_{d1}s + d_{d0}} \tag{4-2}$$

The state and output equations of Eq. (4-1) can be expressed by the equations below:

$$\dot{x} = A_d x + B_d d_0 \tag{4-3}$$

$$d = C_d x \tag{4-4}$$

where

$$A_d = \begin{bmatrix} 0 & 1 & 0 & \cdots & 0 \\ 0 & 0 & 1 & \cdots & 0 \\ \vdots & \vdots & \vdots & & \vdots \\ 0 & 0 & 0 & \cdots & 1 \\ -d_{d0} & -d_{d1} & -d_{d2} & & -d_{dl-1} \end{bmatrix}$$

$$B_d = \begin{bmatrix} 0 \\ \vdots \\ 0 \\ 1 \end{bmatrix},\ C_d = [n_{d0} \quad n_{d1} \quad n_{d2} \quad \cdots \quad n_{dl-1}]$$

The state and output equations of the discrete time model of disturbances can be expressed by the equations below:

$$\delta x(k) = A_{d\delta} x(k) + B_{d\delta} d_0 \tag{4-5}$$

$$d(k) = C_{d\delta} x(k) \tag{4-6}$$

where

$A_{d\delta} = (A_{dz} - I_l)/T_c$, I_l: 1 × 1 unit matrix

$B_{d\delta} = B_{dz}/T_c$, $C_{d\delta} = C_{dz}$

$A_{dz} = e^{A_d T_c}$, $B_{dz} = \int_0^{T_c} e^{A_d T_c} d\tau \, B_d$

A_{dz}, B_{dz} and C_{dz} are a system/control matrix where Eq. (4-3) or (4-4) is discretized by the z operator each. These can be determined using the discretization method "zoh" or "matched" (matched pole-zero model [5]) using the MATLAB® function "c2dm". Note that the matched pole-zero model has the same poles as those of the step invariant model.

From Eqs. (4-5) and (4-6), the transfer function $G_d(\delta)$ of the discrete time model of disturbances can be expressed by the equations below:

$$G_d(\delta) = C_{d\delta}(\delta I_l - A_{d\delta})^{-1} B_{P\delta} = \frac{n_d(\delta)}{d_d(\delta)} = \frac{n_{dl-1}\delta^{l-1} + \cdots n_{d1}\delta + n_{d0}}{\delta^l + d_{dl-1}\delta^{l-1} + \cdots d_{d1}\delta + d_{d0}} \tag{4-7}$$

Note that the numerator polynomial of the disturbance model $n_d(\delta)$ will not be used for compensator design.

4.1.3 Coprime Factorization of Compensator Design Model

To get ready for designing the compensator based on the parametrization of the stabilizing compensator, the compensator design model of Eq. (3-4) is expressed by the coprime factorization below. If the controlled object is a system with multiple inputs/outputs, the model needs to be expressed in right and left coprime factorizations. This controlled object is a system with single input/output, which means that the right coprime factorization is identical to the left coprime factorization. Therefore, this report simply uses the term "coprime factorization".

$$P(\delta) = N_P(\delta)/D_P(\delta) \tag{5-1}$$

$$N_P(\delta) = \frac{n_P(\delta)}{f(\delta)} = \frac{n_{Pn-1}\delta^{n-1} + \cdots + n_{P1}\delta + n_{P0}}{\delta^n + f_{n-1}\delta^{n-1} + \cdots + f_1\delta + f_0} \tag{5-2}$$

$$D_P(\delta) = \frac{d_P(\delta)}{f(\delta)} = \frac{\delta^n + d_{Pn-1}\delta^{n-1} + \cdots + d_{P1}\delta + d_{P0}}{\delta^n + f_{n-1}\delta^{n-1} + \cdots + f_1\delta + f_0} \tag{5-3}$$

$f(\delta)$ is a stable polynomial and any given parameter that can be set by the designer. When $f(\delta)$ is said to be stable, this means that its root exists at the center of the complex plane $-1/T_c$ within the circle of radius $1/T_c$ (see Fig. 9). How to set $f(\delta)$ will be described later.

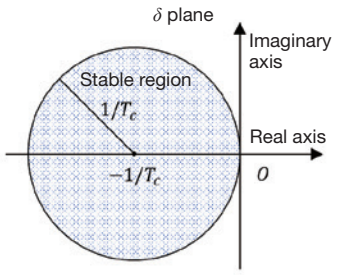

Fig. 9 Stable region of δ operator

4.1.4 Deriving a Compensator

For steering assist control, assume that the compensator $C_r(\delta)$ in Eqs. (1-1) and (1-2) is $C_r(\delta) = 0$. In this case, the control system can be represented by Fig. 10:

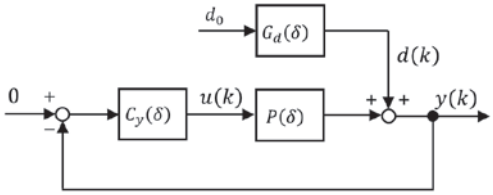

Fig. 10 Block diagram of steering assist control system

The compensator $C_y(\delta)$ based on the parametrization of the stabilizing compensator can be expressed by the equations below:

$$C_y(\delta) = N_C(\delta)/D_C(\delta) \tag{6-1}$$

$$N_C(\delta) = X_P(\delta) + R(\delta)D_P(\delta) \tag{6-2}$$

$$D_C(\delta) = Y_P(\delta) - R(\delta)N_P(\delta) \tag{6-3}$$

$$X_P(\delta) = \frac{n_X(\delta)}{g(\delta)} = \frac{n_{Xn-1}\delta^{n-1} + \cdots + n_{X1}\delta + n_{X0}}{\delta^{n-1} + g_{n-2}\delta^{n-2} + \cdots + g_1\delta + g_0} \tag{6-4}$$

$$Y_P(\delta) = \frac{n_Y(\delta)}{g(\delta)} = \frac{n_{Yn-1}\delta^{n-1} + \cdots + n_{Y1}\delta + n_{Y0}}{\delta^{n-1} + g_{n-2}\delta^{n-2} + \cdots + g_1\delta + g_0} \tag{6-5}$$

$g(\delta)$ is a stable polynomial that is any given parameter to be set by the designer. $R(\delta)$ is a stable-proper transfer function (degree of numerator polynomial is equal to or less than degree of denominator polynomial) that is a free parameter to be selected by the designer. How to set these parameters will be described later.

$X_p(\delta)$ and $Y_p(\delta)$ are solutions to Bezout equations.

$$X_P(\delta)N_P(\delta) + Y_P(\delta)D_P(\delta) = 1 \tag{6-6}$$

Firstly, $X_p(\delta)$ and $Y_p(\delta)$ should be derived. Multiplying both sides of Eq. (6-6) by $h(\delta) = f(\delta)g(\delta)$ yields an identical equation below:

$$n_X(\delta)n_P(\delta) + n_Y(\delta)d_p(\delta) = h(\delta) \tag{6-7}$$

where

$$h(\delta) = \delta^{2n-1} + h_{2n-2}\delta^{2n-2} + \ldots + h_1\delta + h_0$$

When $n_p(\delta)$ and d_p (δ) do not share a common divisor, $n_x(\delta)$ and $n_y(\delta)$ that satisfy Eq. (6-7) will be uniquely decided. Their coefficient can be determined using the equation below [5]:

$$\Theta^T = \Psi^T E^{-1} \tag{6-8}$$

where

$$\Theta^T = [n_{Y0} \ \cdots \ n_{Yn-1} \ n_{X0} \ \cdots \ n_{Xn-1}]$$
$$\Psi^T = [h_0 \ h_1 \ \cdots \ h_{2n-2} \ 1]$$
$$E = \begin{bmatrix} d_{P0} & d_{P1} & \cdots & d_{Pn-1} & 1 & 0 & \cdots & 0 & 0 \\ 0 & d_{P0} & \cdots & d_{Pn-2} & d_{Pn-1} & 1 & \cdots & 0 & 0 \\ \vdots & \vdots & & \vdots & \vdots & \vdots & & \vdots & \vdots \\ 0 & 0 & \cdots & d_{P0} & d_{P1} & d_{P2} & \cdots & d_{Pn-1} & 1 \\ n_{P0} & n_{P1} & \cdots & n_{Pn-1} & 0 & 0 & \cdots & 0 & 0 \\ 0 & n_{P0} & \cdots & n_{Pn-2} & n_{Pn-1} & 0 & \cdots & 0 & 0 \\ \vdots & \vdots & & \vdots & \vdots & \vdots & & \vdots & \vdots \\ 0 & 0 & \cdots & n_{P0} & n_{P1} & n_{P2} & \cdots & n_{Pn-1} & 0 \end{bmatrix}$$

Next is the process to derive $R(\delta)$. In Fig. 10, the control output $y(k)$ in response to the disturbance $d(k)$ can be expressed by the equation below:

$$y(k) = S(\delta)d(k) = D_C(\delta)D_P(\delta)G_d(\delta)d_0 \tag{7-1}$$

$G_d(\delta)$ may have unstable poles or a pole that can delay the attenuation of $d(k)$ regardless of its stability. In order to minimize fluctuations of $y(k)$ due to the effect of such poles as quickly as possible, the zero of $D_c(\delta)$ (the root of the numerator polynomial) must include the poles of $G_d(\delta)$. Therefore, it is necessary to select $R(\delta)$ so that the numerator polynomial of $D_c(\delta)$ includes the denominator polynomial $d_d(\delta)$ of $G_d(\delta)$. Since the degree of the disturbance model of Eq. (4-7) is l, the degree of $R(\delta)$ is set to l-1. $R(\delta)$ is expressed by the equation below:

$$R(\delta) = \frac{n_R(\delta)}{d_R(\delta)} = \frac{n_{Rl-1}\delta^{l-1} + n_{Rl-2}\delta^{l-2} + \cdots + n_{R1}\delta + n_{R0}}{\delta^{l-1} + d_{Rl-2}\delta^{l-2} + \cdots + d_{R1}\delta + d_{R0}} \tag{7-2}$$

where $d_R(\delta)$ is a stable polynomial. How to set the polynomial will be described later.

Developing $D_c(\delta)$ yields the equation below:

$$D_C(\delta) = Y_P(\delta) - R(\delta)N_P(\delta) = \frac{n_Y(\delta)}{g(\delta)} - \frac{n_R(\delta)}{d_R(\delta)}\frac{n_P(\delta)}{f(\delta)} = \frac{d_R(\delta)f(\delta)n_Y(\delta) - g(\delta)n_P(\delta)n_R(\delta)}{d_R(\delta)f(\delta)g(\delta)} \tag{7-3}$$

The following identical equation should be set so that the numerator polynomial of Eq. (7-3) includes $d_d(\delta)$:

$$d_R(\delta)f(\delta)n_Y(\delta) - g(\delta)n_P(\delta)n_R(\delta) = d_d(\delta)q(\delta) \tag{7-4}$$

Modifying Eq. (7-4) yields the equation below:

$$d_d(\delta)q(\delta) + w(\delta)n_R(\delta) = \gamma(\delta) \tag{7-5}$$

where

$$w(\delta) = g(\delta)n_P(\delta) = \delta^{2n-2} + w_{2n-3}\delta^{2n-3} + \ldots + w_1\delta + w_0$$
$$\gamma(\delta) = d_R(\delta)f(\delta)n_Y(\delta) = \delta^{2n+l-2} + \gamma_{2n+l-3}\delta^{2n+l-3} + \ldots + \gamma_1\delta + \gamma_0$$
$$q(\delta) = q_{2n-2}\delta^{2n-2} + q_{2n-3}\delta^{2n-3} + \ldots + q_1\delta + q_0$$

The coefficient of $n_R(\delta)$ can be determined using the equation below:

$$\Theta^T = \Psi^T E^{-1} \tag{7-6}$$

where

$$\Theta^T = [q_0 \ q_1 \ \cdots \ q_{2n-2} \ n_{R0} \ n_{R1} \ \cdots \ n_{Rl-1}]$$
$$\Psi^T = [\gamma_0 \ \gamma_1 \ \cdots \ \gamma_{2n+l-3} \ 1]$$
$$E = \begin{bmatrix} E_1 \\ E_2 \end{bmatrix}$$
$$E_1 = \begin{bmatrix} d_{d0} & d_{d1} & \cdots & d_{dl-1} & 1 & 0 & \cdots & 0 & 0 \\ 0 & d_{d0} & \cdots & d_{dl-2} & d_{dl-1} & 1 & \cdots & 0 & 0 \\ \vdots & \vdots & & \vdots & \vdots & \vdots & & \vdots & \vdots \\ 0 & 0 & \cdots & d_{d0} & d_{d1} & d_{d2} & \cdots & d_{dl-1} & 1 \end{bmatrix}$$
: $(2n-1)\times(2n+l-1)$ matrix
$$E_2 = \begin{bmatrix} w_0 & w_1 & \cdots & w_{2n-2} & 0 & \cdots & 0 & \cdots & 0 \\ 0 & w_0 & \cdots & w_{2n-3} & w_{2n-2} & \cdots & 0 & \cdots & 0 \\ \vdots & \vdots & & \vdots & \vdots & & \vdots & & \vdots \\ 0 & 0 & \cdots & w_0 & w_2 & \cdots & w_{2n-2} & \cdots & 0 \end{bmatrix}$$
: $l\times(2n+l-1)$ matrix

4.1.5 Example of Basic Design of Compensator

(1) Determining the compensator design model

When A_p, B_p, C_p, E_p, and F_p in Eqs. (2-3) and (2-4) are given their physical parameter values and then discretized, the transfer function of Eq. (3-3) will be:

$$P(\bar{\delta}) = \frac{n_P(\bar{\delta})}{d_P(\bar{\delta})} = \frac{n_{P1}\bar{\delta} + n_{P0}}{\bar{\delta}^2 + d_{P1}\bar{\delta} + d_{P0}} = \frac{7.807\times10^{-3}(\bar{\delta} + 1.980)}{\bar{\delta}^2 + 7.964\times10^{-2}\bar{\delta} + 2.163\times10^{-2}} \tag{8-1}$$

The δ operator and the coefficients of the numerator and denominator of Eq. (8-1) were made dimensionless with the inverse of the control period $1/T_c$ (hereinafter "the control frequency"). In other words, $\bar{\delta}$ in the equation is $\bar{\delta} = T_c\delta$. All figures appearing in the following examples indicate dimensionless transfer functions.

The poles and zeros of Eq. (8-1) are all within the stable region, implying a stable controlled object. Note that the zeros in Eq. (8-1) have been added through discretization.

Next, the coprime factorization of Eq. (8-1) $P(\bar{\delta}) = N_p(\bar{\delta}) / D_p(\bar{\delta})$ is set as follows:

$$N_P(\bar{\delta}) = \frac{n_P(\bar{\delta})}{f(\bar{\delta})} = \frac{7.807\times10^{-3}(\bar{\delta} + 1.980)}{(\bar{\delta} + 0.2583)^2} \tag{8-2}$$

$$D_P(\bar{\delta}) = \frac{d_P(\bar{\delta})}{f(\bar{\delta})} = \frac{\bar{\delta}^2 + 7.964\times10^{-2}\bar{\delta} + 2.163\times10^{-2}}{(\bar{\delta} + 0.2583)^2} \tag{8-3}$$

$1/f(\bar{\delta})$ in Eqs. (8-2) and (8-3) is the matched pole-zero model of the following stable transfer function $1/f(s)$ that has been made dimensionless with the control frequency $1/T_c$:

$$1/f(s) = 1/(s^2 + 2\zeta_f\omega_f s + \omega_f^2) \tag{8-4}$$

where $0 < \omega_f$, $0 < \zeta_f$

If $1/f(s)$ is stable, its matched pole-zero model $1/f(\bar{\delta})$is also stable. To allow the control system to deliver high responsivity, it is desirable to set ω_f to a value as high as possible. ζ_f, which is the attenuation factor of the poles of the control system, should be set to 1 or more. For convenience, these are set as follows:

$\zeta_f = 1$, $\omega_f = 2\sqrt{K_{pe}/I_{pe}}$ (natural angular frequency decided by the equivalent stiffness and equivalent inertia moment of the pinion shaft multiplied by 2).

The solutions to Bezout equations $X_p(\delta)$ and $Y_p(\delta)$ can be expressed in the equations below:

$$X_P(\bar{\delta}) = \frac{n_X(\bar{\delta})}{g(\bar{\delta})} = \frac{8.179\bar{\delta} + 0.2314}{\bar{\delta} + 0.2583} \tag{8-5}$$

$$Y_P(\bar{\delta}) = \frac{n_Y(\bar{\delta})}{g(\bar{\delta})} = \frac{\bar{\delta} + 0.6314}{\bar{\delta} + 0.2583} \tag{8-6}$$

$1/g(\delta)$ in Eqs. (8-5) and (8-6) is the matched pole-zero model of the following stable transfer function $1/g(s)$ that has been made dimensionless with the control frequency $1/T_c$:

$$1/g(s) = 1/(s + \omega_g) \tag{8-7}$$

where $\omega_g = 2\sqrt{K_{TB}/I_{pe}}$ is used.

(2) Setting disturbance models

The disturbance model for the continuous time system is set as follows. The numerator polynomial $n_d(s)$ of the disturbance model is hereinafter omitted because it will not be used for compensator design.

$$G_d(s) = \frac{n_d(s)}{d_d(s)} = \frac{n_d(s)}{s^2 + 2\zeta_d\omega_d s + \omega_d{}^2} \tag{9-1}$$

where $\zeta_d = 1$. The following settings will be used according to the steering assist torque level:

$\omega_d = 0.5\sqrt{K_{pe}/I_{pe}}$: Large steering assist torque
$\omega_d = 0.9\sqrt{K_{pe}/I_{pe}}$: Medium steering assist torque
$\omega_d = 1.5\sqrt{K_{pe}/I_{pe}}$: Small steering assist torque

In these settings, the step invariant or matched pole-zero model of the transfer function in Eq. (9-1) that has been made dimensionless with the control frequency $1/T_c$ can be expressed by the equation below:

$$G_d(\bar{\delta}) = \frac{n_d(\bar{\delta})}{d_d(\bar{\delta})} = \frac{n_d(\bar{\delta})}{\bar{\delta}^2 + 2\zeta_d\bar{\omega}_d\bar{\delta} + \omega_d{}^2} = \frac{n_d(\bar{\delta})}{(\bar{\delta} + \bar{\omega}_d)^2} \tag{9-2}$$

where $\zeta_d = 1$. $\bar{\omega}_d$ is as follows:

$\bar{\omega}_d = 0.07198$: Large steering assist torque
$\bar{\omega}_d = 0.1258$: Medium steering assist torque
$\bar{\omega}_d = 0.2008$: Small steering assist torque

(3) Deriving free parameter $R(\bar{\delta})$

It is assumed that the pole $d_R(\bar{\delta})$ of the free parameter is the same as $g(\bar{\delta})$ of Eqs. (8-5) and (8-6). Substituting Eqs. (8-2), (8-6), and (9-2) as well as $d_R(\bar{\delta}) = g(\bar{\delta}) = \bar{\delta} + 0.2583$ in Eq. (7-6) yields the following free parameter $R(\delta)$:

$$R(\bar{\delta}) = \frac{n_R(\bar{\delta})}{d_R(\bar{\delta})} = \frac{\bar{n}_{R1}\bar{\delta} + \bar{n}_{R0}}{\bar{\delta} + 0.2583} \tag{9-3}$$

where

$\left.\begin{aligned}\bar{n}_{R1} &= 15.640\\ \bar{n}_{R0} &= 2.429\end{aligned}\right\}$: Large steering assist torque

$\left.\begin{aligned}\bar{n}_{R1} &= 10.135\\ \bar{n}_{R0} &= 1.888\end{aligned}\right\}$: Medium steering assist torque

$\left.\begin{aligned}\bar{n}_{R1} &= 3.747\\ \bar{n}_{R0} &= 0.8549\end{aligned}\right\}$: Small steering assist torque

(4) Frequency characteristics of control system

From the above, substituting Eqs. (8-2), (8-3), (8-5), (8-6), and (9-3) in Eqs. (6-1) to (6-3) yields $C_y(\delta)$ as follows:

$$C_y(\bar{\delta}) = \frac{23.819(\bar{\delta} + 0.121)(\bar{\delta}^2 + 0.2204\bar{\delta} + 2.358\times10^{-2})}{(\bar{\delta} + 0.8819)(\bar{\delta} + 0.07198)^2}$$

: Large steering assist torque (10-1)

$$C_y(\bar{\delta}) = \frac{18.314(\bar{\delta} + 0.1513)(\bar{\delta}^2 + 0.2392\bar{\delta} + 2.031\times10^{-2})}{(\bar{\delta} + 0.8172)(\bar{\delta} + 0.1258)^2}$$

: Medium steering assist torque (10-2)

$$C_y(\bar{\delta}) = \frac{11.926(\bar{\delta} + 0.205)(\bar{\delta} + 0.1938)(\bar{\delta} + 0.07162)}{(\bar{\delta} + 0.7172)(\bar{\delta} + 0.2008)^2}$$

: Small steering assist torque (10-3)

According to the equations above, the poles of $C_y(\delta)$ include the pole $d_d(\bar{\delta})$ of the disturbance model in Eq. (9-2) for all the torque cases. Fig. 11 shows the poles and zeros of the compensator of Eqs. (10-1) to (10-3) plotted on a complex plane. The figure indicates that all the poles and zeros are within the stable region. Note that both the vertical and horizontal axes have been made dimensionless with the control frequency $1/T_c$.

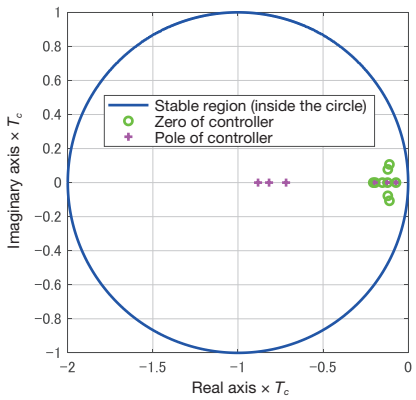

Fig. 11 Poles and zeros of compensator (basic design)

Next, the frequency characteristics of $C_y(\bar{\delta})$, $C_y(\bar{\delta})P(\bar{\delta})$ (loop transfer function), and $S(\bar{\delta})$ are shown in Fig. 12. For plotting of the Bode diagrams in Fig. 12, $C_y(\bar{\delta})$, $C_y(\bar{\delta})P(\bar{\delta})$, and $S(\bar{\delta})$ have been converted into the form of the z operator and applied with the MATLAB® function "dbode". The horizontal axis of these diagrams has been made dimensionless with the control frequency $1/T_c$. According to the diagrams, the gain of the compensator or loop transfer function depends on the steering assist torque level.

This design approach is not intended to design compensators with a focus on the loop transfer function or stability margin. Still, it should be noted that eventually the

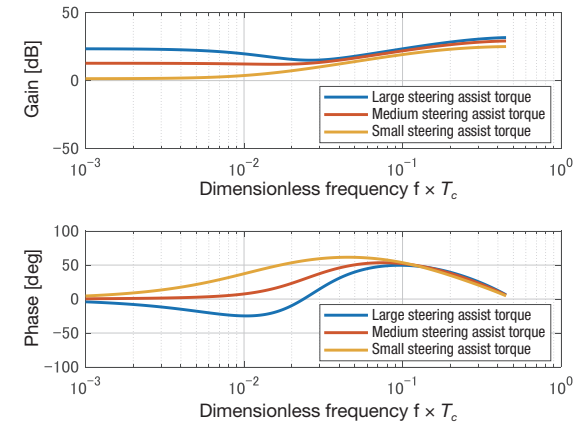

(a) Frequency characteristics of compensator Cy(δ)

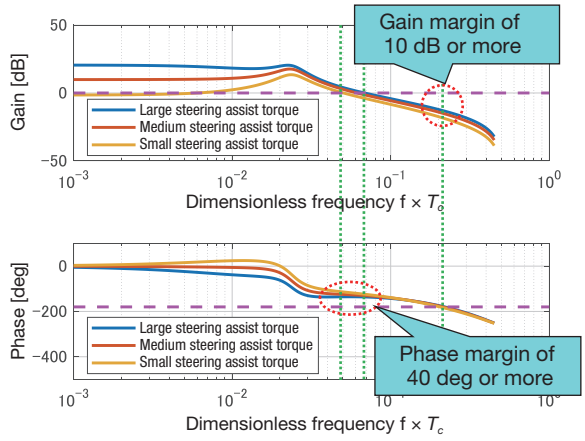

(b) Frequency characteristics of loop transfer function Cy(δ) P(δ)

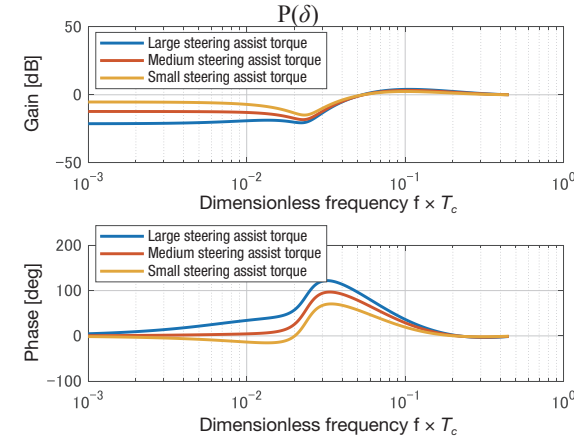

(c) Frequency characteristics of transfer function S(δ)

Fig. 12 Frequency characteristics of steering assist control system

gain margin is not less than 10 dB and the phase margin not less than 40 degrees for all cases.

$S(\bar{\delta})$, which is called the sensitivity function, is less likely to be affected by the parameter variations of the controlled object or disturbances with its smaller gain. The smaller gain means a smaller control output to the steering wheel rotation, in other words, a larger steering assist torque. The poles of $S(\bar{\delta})$ are the poles $d_{cl}(\bar{\delta})$ of the closed-loop transfer function of the control system in Fig. 10 and can be expressed by the equation below:

$$d_{cl}(\bar{\delta}) = \{f(\bar{\delta})\}^2 g(\bar{\delta}) d_R(\bar{\delta}) = (\bar{\delta} + 0.2583)^6 \quad (10\text{-}4)$$

That is, $f(\bar{\delta})$, $g(\bar{\delta})$ and $d_R(\bar{\delta})$ that were set during design become the poles of the closed-loop transfer function. This implies that this design approach is to design a compensator by setting the poles of the closed-loop transfer function (or poles of the control system).

4.2 Basic Design of Steering Angle Control Compensator

4.2.1 Deriving a Compensator Design Model

Fig. 13 shows a model of EPS including the steering wheel. For steering angle control, the steering angle determined from the motor rotation angle must follow the target steering angle signal while suppressing vibration caused by the turn of the steering wheel. Therefore, the controlled object is the steering system including the rotary motion of the equivalent inertia moment of the steering wheel shaft. The figure uses symbols to indicate the following meaning. The other symbols not on the list below have the same meaning as those used in Fig. 8.

θ_m : Motor rotation angle [rad] ($\theta_m = R_P \theta_P$)

I_h : Equivalent inertia moment of steering wheel shaft [kg·m^2]

C_h : Equivalent viscous resistance coefficient of steering wheel shaft [N·m/(rad/s)]

τ_h : Steering wheel input torque [N·m] (assume $\tau_h = 0$ with the driver's hands off the wheel)

The control output, namely, the steering angle signal $\hat{\theta}_p$ can be determined using the equation below:

$$\hat{\theta}_p = \theta_m / R_w \quad (11\text{-}1)$$

Assuming again that i_m is equal to u (the actual current completely follows the motor current command) and that all the parts except the torsion bar are rigid bodies, the rotary motion of the pinion can be expressed by the differential equation below:

$$I_{pe}\ddot{\theta}_p + C_{pe}\dot{\theta}_p = R_w K_t i_m + K_{TB}(\theta_h - \theta_p) - K_r R_p^2 \theta_p \quad (11\text{-}2)$$

where

$i_m = u$

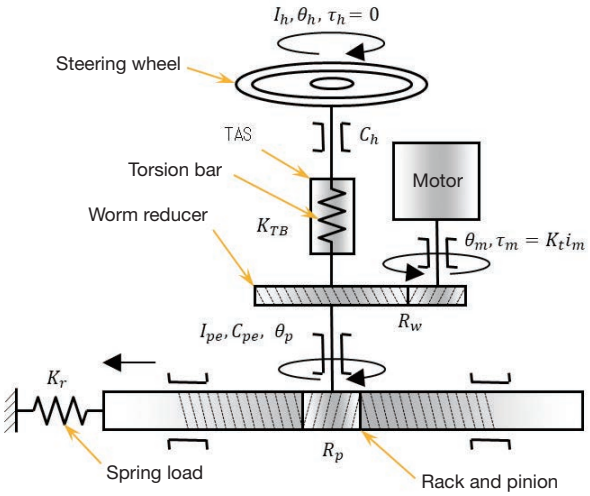

Fig. 13 Model of EPS including steering wheel

The rotary motion of the wheel can be expressed by the equation below:

$$I_h\ddot{\theta}_h + C_h\dot{\theta}_h = -K_{TB}(\theta_h - \theta_p) \quad (11\text{-}3)$$

From Eqs. (11-1) to (11-3), the following state and output equations can be obtained:

$$\dot{x} = A_P x + B_P u \quad (11\text{-}4)$$

$$y = C_P x \quad (11\text{-}5)$$

where

$x = [\theta_p \quad \theta_h \quad \dot{\theta}_p \quad \dot{\theta}_h]^T$: State variable

$y = \hat{\theta}_p = \theta_m / R_w = \theta_p$: Control output

$$A_P = \begin{bmatrix} 0 & 0 & 1 & 0 \\ 0 & 0 & 0 & 1 \\ -K_{pe}/I_{pe} & K_{TB}/I_{pe} & -C_{pe}/I_{pe} & 0 \\ K_{TB}/I_h & -K_{TB}/I_h & 0 & -C_h/I_h \end{bmatrix}$$

$$B_P = \begin{bmatrix} 0 \\ 0 \\ R_w K_t / I_{pe} \\ 0 \end{bmatrix}, \quad C_P = [1 \quad 0 \quad 0 \quad 0]$$

In Eqs. (11-4) and (11-5), the state and output equations for the discrete time model can be expressed by the equations below:

$$\delta x(k) = A_{P\delta} x(k) + B_{P\delta} u(k) \quad (11\text{-}6)$$

$$y(k) = C_{P\delta} x(k) \quad (11\text{-}7)$$

where

$A_{P\delta} = (A_{Pz} - I_4)/T_c$, I_4 : 4 × 4 unit matrix

$B_{P\delta} = B_{Pz}/T_c$, $C_{P\delta} = C_{Pz} = C_P$

$A_{Pz} = e^{A_P T_c}$, $B_{Pz} = \int_0^{T_c} e^{A_P T_c} d\tau \, B_P$

When Eqs. (11-6) and (11-7) are selected as the compensator design model, the transfer function $P(\delta)$ in Figs. 5 and 6 can be expressed by the equation below:

$$P(\delta) = C_{P\delta}(\delta I_4 - A_{P\delta})^{-1} B_{P\delta} = \frac{n_P(\delta)}{d_P(\delta)} = \frac{n_{P3}\delta^3 + n_{P2}\delta^2 n_{P1}\delta + n_{P0}}{\delta^4 + d_{P3}\delta^3 + d_{P2}\delta^2 + d_{P1}\delta + d_{P0}} \quad (11\text{-}8)$$

The setting of disturbance models and coprime factorization of the compensator design model are omitted here as these are as described in sections 4.1.2 and 4.1.3. The following describes how to derive a compensator.

4.2.2 Setting a Target Value Signal Model

This section discusses the target value signal model of degree l represented by the equation below:

$$G_r(\delta) = \frac{n_r(\delta)}{d_r(\delta)} = \frac{n_{dl-1}\delta^{l-1} + \cdots n_{d1}\delta + n_{d0}}{\delta^l + d_{dl-1}\delta^{l-1} + \cdots d_{d1}\delta + d_{d0}} \quad (12)$$

Note that the numerator polynomial of the target value signal model $n_r(\delta)$ will not be used for compensator design.

4.2.3 Deriving a Compensator

For steering angle control, assume that the compensator $C_r(\delta)$ of Eqs. (1-1) and (1-2) is $C_r(\delta) = F_c(\delta) / D_c(\delta)$ based on the parametrization [3] of the stabilizing compensator for the two-degree-of-freedom control system. $F_c(\delta)$ is a stable-proper transfer function (hereinafter a "pre-compensator"). In this case, the control system can be represented by Fig. 14:

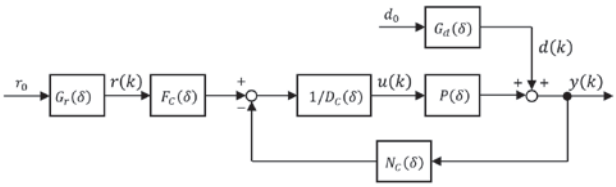

Fig. 14 Block diagram of steering angle control system

In the control system shown in Fig. 14, the transfer function $G_{ry}(\delta)$ ranging from the target steering angle signal $r(k)$ to the control output y (hereinafter "target tracking characteristics") can be expressed by the equation below:

$$G_{ry}(\delta) = F_C(\delta) N_P(\delta) \quad (13\text{-}1)$$

Then, $G_{ry}(\delta)$ is set as follows:

$$G_{ry}(\delta) = \frac{n_M(\delta)}{d_M(\delta)} = \frac{n_{Mm-1}\delta^{m-1} + n_{Mm-2}\delta^{m-2} + \cdots + n_{M1}\delta + n_{M0}}{\delta^m + d_{Mm-1}\delta^{m-1} + \cdots + d_{M1}\delta + d_{M0}} \quad (13\text{-}2)$$

where $d_M(\delta)$ is a stable polynomial.

Next, the deviation $e_r(k)$ of the output $y_r(k)$ of $G_{ry}(\delta)$ from $r(k)$ can be expressed by the equation below:

$$\begin{aligned} e_r(k) &= r(k) - y_r(k) = r(k) - G_{ry}(\delta) r(k) \\ &= \{1 - G_{ry}(\delta)\} r(k) = \frac{d_M(\delta) - n_M(\delta)}{d_M(\delta)} r(k) \\ &= \frac{d_M(\delta) - n_M(\delta)}{d_M(\delta)} G_r(\delta) r_0 \end{aligned} \quad (13\text{-}3)$$

$d_M(\delta)$'s degree m may be any number, but needs to be set from the following perspectives:

① If the compensator design model has an unstable zero, in other words, if $n_p(\delta)$ or $d_r(\delta)$ has an unstable root, $n_M(\delta)$ must include the root.

② In order for the deviation $e_r(k)$ to converge to zero (0) asymptotically, $\{d_M(\delta) - n_M(\delta)\}$ in Eq. (13-3) must have the unstable pole of $G_r(\delta)$ as its root.

Then, assuming that $n_p(\delta)$ has an unstable root, an identical equation shown below is set so that $\{d_M(\delta) - n_M(\delta)\}$ in Eq. (13-3) has the pole $d_r(\delta)$ of Eq. (12) as a divisor:

$$d_M(\delta) - n_P(\delta)\beta_M(\delta) = d_r(\delta)\alpha_M(\delta) \quad (13\text{-}4)$$

where

$$n_M(\delta) = n_P(\delta)\beta_M(\delta) \quad (13\text{-}5)$$

$\alpha_M(\delta)$ and $\beta_M(\delta)$ are polynomials of degree n-1 and l-1, respectively. Degree of $d_M(\delta)$ is $m = n + l - 1$. Modifying Eq. (13-4) gives the equation below:

$$n_P(\delta)\beta_M(\delta) + d_r(\delta)\alpha_M(\delta) = d_M(\delta) \quad (13\text{-}6)$$

The coefficient of $\beta_M(\delta)$ can be determined using the equation below:

$$\Theta^T = \Psi^T E^{-1} \quad (13\text{-}7)$$

where

$$\Theta^T = [\alpha_{M0} \ \cdots \ \alpha_{Mn-1} \ \beta_{M0} \ \cdots \ \beta_{Ml-1}]$$
$$\Psi^T = [d_{M0} \ d_{M1} \ \cdots \ d_{Mn+l-2} \ 1]$$
$$E = \begin{bmatrix} E_1 \\ E_2 \end{bmatrix}$$
$$E_1 = \begin{bmatrix} d_{r0} & d_{r1} & \cdots & d_{rl-1} & 1 & 0 & \cdots & 0 & 0 \\ 0 & d_{r0} & \cdots & d_{rl-2} & d_{rl-1} & 1 & \cdots & 0 & 0 \\ \vdots & \vdots & & \vdots & \vdots & \vdots & & \vdots & \vdots \\ 0 & 0 & \cdots & d_{r0} & d_{r1} & d_{r2} & \cdots & d_{rl-1} & 1 \end{bmatrix}$$
: $n \times (n+l)$ matrix
$$E_2 = \begin{bmatrix} n_{P0} & n_{P1} & \cdots & n_{Pn-1} & 0 & \cdots & 0 & \cdots & 0 \\ 0 & n_{P0} & \cdots & n_{Pn-2} & n_{Pn-1} & \cdots & 0 & \cdots & 0 \\ \vdots & \vdots & & \vdots & \vdots & & \vdots & & \vdots \\ 0 & 0 & \cdots & n_{P0} & n_{P2} & \cdots & n_{Pn-1} & \cdots & 0 \end{bmatrix}$$
: $l \times (n+l)$ matrix

How to set $d_M(\delta)$ will be described later.

Substituting Eq. (13-2) in Eq. (13-1) and modifying it gives the equation below:

$$F_C(\delta) = \frac{f(\delta) n_M(\delta)}{n_P(\delta) d_M(\delta)} \tag{13-8}$$

Substituting the relation of Eq. (13-5) in Eq. (13-8) yields the equation below:

$$F_C(\delta) = \frac{f(\delta) \beta_M(\delta)}{d_M(\delta)} \tag{13-9}$$

Eq. (13-9) can be used to determine a pre-compensator $F_c(\delta)$.

A description of how to derive the compensator $C_y(\delta)$ is omitted here as it is the same as for steering assist control. The next section provides an example of basic design of the compensator.

4.2.4 Example of Basic Design of Compensator

(1) Determining a compensator design model

When A_p, B_p, C_p, E_p, and F_p in Eqs. (11-4) and (11-5) are input with their physical parameter values, discretized and made dimensionless with the control frequency $1/T_c$, the transfer function of Eq. (11-8) is as follows:

$$P(\bar{\delta}) = \frac{n_P(\bar{\delta})}{d_P(\bar{\delta})} \tag{14-1}$$

where

$$n_P(\bar{\delta}) = 3.406\times10^{-5}(\bar{\delta} + 1.980) \times(\bar{\delta}^2 + 8.741\times10^{-3}\bar{\delta} + 5.718\times10^{-5})$$
$$d_P(\bar{\delta}) = \bar{\delta}(\bar{\delta} + 1.233\times10^{-2}) \times(\bar{\delta}^2 + 7.599\times10^{-2}\bar{\delta} + 2.685\times10^{-2})$$

Fig. 15 shows the poles and zeros of $P(\delta)$ in Eq. (14-1) plotted on a complex plane. With a focus on the numerator of Eq. (14-1), there are three zeros. Of these, a real root is a zero that has been added through discretization. The remaining complex roots correspond to the original continuous time system. These complex roots are what make the resonance point (generally with a low attenuation factor), which is decided by the equivalent inertia moment of the steering wheel shaft and the stiffness of the torsion bar, appear as an antiresonance point in the zeros of $P(\delta)$. Causing either compensator $C_r(\delta)$ or $C_y(\delta)$ to have these zeros as divisors in its poles could prevent the antiresonance point from appearing in the zeros of the transfer characteristics ranging from the target steering angle signal $r(k)$ to the control output $y(k)$. In this case, however, the antiresonance point inevitably appears as a pole of the transfer characteristics from $r(k)$ to the wheel rotation angle to be a resonance point. So, if the target steering angle signal abruptly changes, vibration may occur as the steering wheel is turned. Then, the compensator should be so designed that the poles of the compensator cannot have the zeros of the compensator design model as their divisors. This can be achieved by determining the compensator $F_c(\delta)$ using Eq. (13-9) and making settings so that the denominator polynomial $f(\delta)$ in Eqs. (5-2) and (5-3), the denominator polynomial $g(\delta)$ in Eqs. (6-4) and (6-5), and the denominator polynomial $d_R(\delta)$ in Eq. (7-2) cannot have the zeros of the compensator design model as their divisors.

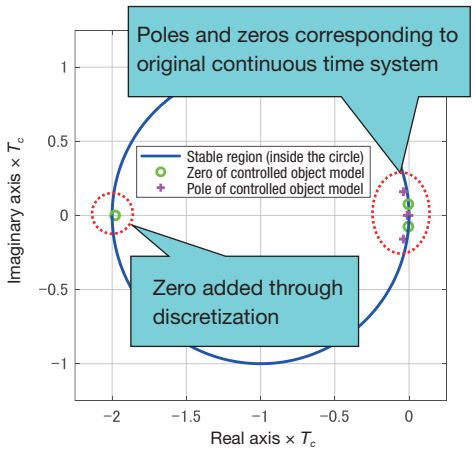

Fig. 15 Poles and zeros of compensator design model

Next is to set the coprime factorization $P(\bar{\delta}) = N_p(\bar{\delta}) / D_p(\bar{\delta})$ in Eq. (14-1) as follows:

$$N_P(\bar{\delta}) = \frac{n_P(\bar{\delta})}{f(\bar{\delta})} \tag{14-2}$$

$$D_P(\bar{\delta}) = \frac{d_P(\bar{\delta})}{f(\bar{\delta})} \tag{14-3}$$

$1/f(\bar{\delta})$ in Eqs. (14-2) and (14-3) are the matched pole-zero model of the following stable transfer function $1/f(s)$ that has been made dimensionless with the control frequency $1/T_c$:

$$1/f(s) = 1/\ \{f_1(s)f_2(s)\} \tag{14-4}$$

where

$$f_1(s) = s^2 + 2\zeta_{f1}\omega_{f1}s + \omega_{f1}^2$$
$$f_2(s) = s^2 + 2\zeta_{f2}\omega_{f1}s + \omega_{f2}^2$$
$$0<\omega_{f1},\quad 0<\omega_{f2},\quad 0<\zeta_{f1},\quad 0<\zeta_{f2}$$

where $\zeta_{f1} = \zeta_{f2} = 2.3$ and $\omega_{f1} = \omega_{f2} = 0.7\sqrt{K_{pe}/I_{pe}}$.
Reducing ζ_{f1} and ζ_{f2} or raising ω_{f1} and ω_{f2} will tend to cause the controller to have unstable poles. So, these parameters are set to smaller values than for steering assist control.

The solutions to Bezout equations $X_p(\bar{\delta})$ and $Y_p(\bar{\delta})$ can be expressed by the equations below:

$$X_P(\bar{\delta}) = \frac{n_X(\bar{\delta})}{g(\bar{\delta})} \tag{14-5}$$

$$Y_P(\bar{\delta}) = \frac{n_Y(\bar{\delta})}{g(\bar{\delta})} \tag{14-6}$$

where

$$n_X(\bar{\delta}) = 1910.8(\bar{\delta} + 0.4936) \times (\bar{\delta}^2 + 2.550\times10^{-2}\bar{\delta} + 1.781\times10^{-4})$$
$$n_Y(\bar{\delta}) = (\bar{\delta} + 0.5236)(\bar{\delta} + 0.5953) \times (\bar{\delta} + 1.284\times10^{-3})$$
$$g(\bar{\delta}) = (\bar{\delta} + 2.364\times10^{-2})(\bar{\delta} + 9.930\times10^{-2}) \times (\bar{\delta} + 0.3669)$$

$1/g(\bar{\delta})$ is the matched pole-zero model of the following stable transfer function $1/g(s)$ that has been made dimensionless with the control frequency $1/T_c$:

$$1/g(s) = 1/\ \{g_1(s)g_2(s)\} \tag{14-7}$$

where

$$g_1(s) = s + \omega_{g1}$$
$$g_2(s) = s^2 + 2\zeta_{g2}\omega_{g1}s + {\omega_{g2}}^2$$

where $\zeta_{g2} = 2.3$, $\omega_{g1} = \omega_{g2} = 0.7\sqrt{K_{TB}/I_{pe}}$.

(2) Setting target value signal models

To ensure that the control output tracking to the target steering angle signal, which changes in ramp rate, converges to zero (0) asymptotically, a target value signal model is set as follows:

$$G_r(\bar{\delta}) = \frac{n_r(\bar{\delta})}{d_r(\bar{\delta})} = \frac{1}{\bar{\delta}^2} \tag{15}$$

(3) Setting disturbance models

To ensure that the control output tracking disturbances, which change in ramp rate, converges to zero (0) asymptotically, a disturbance model for the continuous time system is set as follows:

$$G_d(s) = \frac{n_d(s)}{d_d(s)} = \frac{1}{s^2} \tag{16-1}$$

A step invariant model or matched pole-zero model of the transfer function of Eq. (16-1) that has been made into a dimensionless transfer function with the control frequency $1/T_c$ can be expressed by the equation below:

$$G_d(\bar{\delta}) = \frac{n_d(\bar{\delta})}{d_d(\bar{\delta})} = \frac{1}{\bar{\delta}^2} \tag{16-2}$$

(4) Deriving free parameter $R(\bar{\delta})$

It is assumed that the pole $d_R(\bar{\delta})$ of the free parameter is $d_R(\bar{\delta}) = \bar{\delta} + 9.930 \times 10\text{-}2$, which is the same as one of the divisors of $g(\bar{\delta})$ in Eqs. (14-5) and (14-6). Substituting Eqs. (14-2), (14-6) and (15-2) as well as $d_R(\bar{\delta})$ in Eq. (7-6) gives the following free parameter $R(\bar{\delta})$:

$$R(\bar{\delta}) = \frac{n_R(\bar{\delta})}{d_R(\bar{\delta})} = \frac{6590\bar{\delta} - 9.002}{\bar{\delta} + 9.930\times10^{-2}} \tag{16-3}$$

(5) Deriving compensator $F_c(\bar{\delta})$

The target tracking characteristics are set as follows:

$$G_{ry}(\bar{\delta}) = \frac{n_M(\bar{\delta})}{d_M(\bar{\delta})} = \frac{n_P(\bar{\delta})\beta_M(\bar{\delta})}{d_M(\bar{\delta})} \tag{16-4}$$

where

$$n_M(\bar{\delta}) = 1.601\times10^{-3}(\bar{\delta} + 8.925\times10^{-3}) \times (\bar{\delta} + 1.980)(\bar{\delta}^2 + 8.741\bar{\delta} + 5718)$$
$$d_M(\bar{\delta}) = (\bar{\delta} + 4.383\times10^{-2})^5$$

$1/d_M(\delta)$ in Eq. (16-4) is the matched pole-zero model of the following stable transfer function $1/\ d_M(s)$ that has been made dimensionless with the control frequency $1/Tc$:

$$1/d_M(s) = 1/\ \{d_{M1}(s)d_{M2}(s)d_{M3}(s)\} \tag{16-5}$$

where

$$d_{M1}(s) = s + \omega_{M1}$$
$$d_{M2}(s) = s^2 + 2\zeta_{M2}\omega_{M1}s + {\omega_{M2}}^2$$
$$d_{M3}(s) = s^2 + 2\zeta_{M3}\omega_{M3}s + {\omega_{M3}}^2$$
$$0 < \omega_{M1},\ \ 0 < \omega_{M2},\ \ 0 < \omega_{M3},\ \ 0 < \zeta_{M2},\ \ 0 < \zeta_{M3}$$

where $\zeta_{M2} = \zeta_{M3} = 1$ and $\omega_{M1} = \omega_{M2} = \omega_{M3} = 0.3 \text{ x } \sqrt{K_{pe}/I_{pe}}$.
$\beta_M(\bar{\delta})$ in Eq. (16-4) has been determined by substituting $n_p(\bar{\delta})$ of Eq. (14-1), $d_r(\bar{\delta})$ of Eq. (15), and $d_M(\bar{\delta})$ of Eq. (17-2) in Eq. (13-7).

When $f(\bar{\delta})$ of Eqs. (14-2) and (14-3) and $\beta_M(\bar{\delta})$ and $d_M(\bar{\delta})$ of Eq. (16-4) are substituted in Eq. (13-9), the compensator $F_c(\bar{\delta})$ can be expressed by the equation below:

$$F_C(\bar{\delta}) = \frac{n_F(\bar{\delta})}{d_F(\bar{\delta})} \tag{16-6}$$

where

$$n_F(\bar{\delta}) = 46.993(\bar{\delta} + 8.925\times10^{-3}) \times (\bar{\delta} + 2.364\times10^{-2})^2(\bar{\delta} + 0.3669)^2$$
$$d_F(\bar{\delta}) = (\bar{\delta} + 4.383\times10^{-2})^5$$

(6) Frequency characteristics of control system

From the above, substituting Eqs. (14-2), (14-3), (14-5), (14-6), and (16-3) in Eqs. (6-1) to (6-3) yields $C_y(\bar{\delta})$ as follows:

$$C_y(\bar{\delta}) = N_C(\bar{\delta})/D_C(\bar{\delta}) \tag{17-1}$$

where

$$N_C(\bar{\delta}) = \frac{n_{NC}(\bar{\delta})}{d_C(\bar{\delta})} \tag{17-2}$$

$$D_C(\bar{\delta}) = \frac{n_{DC}(\bar{\delta})}{d_C(\bar{\delta})} \tag{17-3}$$

$$n_{NC}(\bar{\delta}) = 8500.8(\bar{\delta} + 1.381\times10^{-2}) \times (\bar{\delta}^2 + 0.2211\times10^{-2}\bar{\delta} + 1.974\times10^{-4}) \times (\bar{\delta}^2 + 0.2360\bar{\delta} + 6.286\times10^{-2})$$
$$n_{DC}(\bar{\delta}) = \bar{\delta}^2(\bar{\delta} + 1.107) \times (\bar{\delta}^2 + 0.1766\bar{\delta} + 0.1137)$$
$$d_C(\bar{\delta}) = (\bar{\delta} + 0.2364\times10^{-2})^2 \times (\bar{\delta} + 0.9930\times10^{-2})(\bar{\delta} + 0.3369)^2$$

Next, the frequency characteristics of $C_y(\bar{\delta})$, $C_y(\bar{\delta})P(\bar{\delta})$ (loop transfer function), $S(\bar{\delta})$, and $G_{yr}(\bar{\delta})$ are shown in Fig. 16.

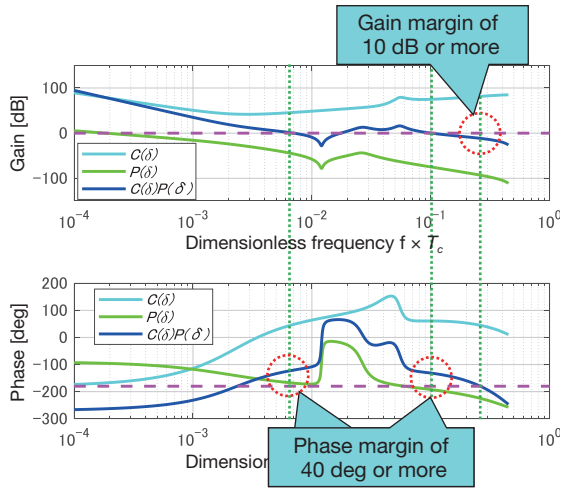

(a) Frequency characteristics of $C_y(\delta)$, $P(\delta)$, and $C_y(\delta)P(\delta)$

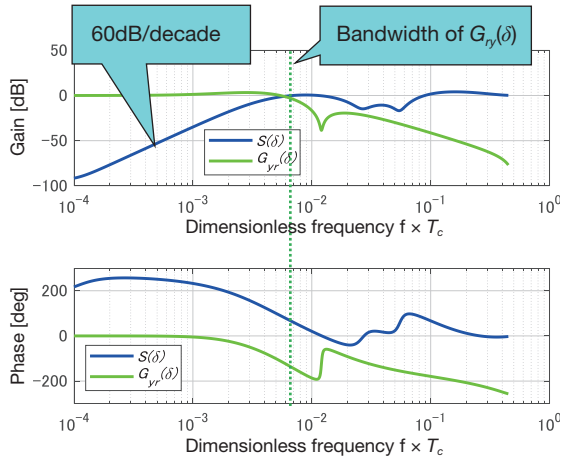

(b) Frequency characteristics of transfer functions $S(\delta)$ and $G_{ry}(\delta)$

Fig. 16 Frequency characteristics of steering angle control system

As a result of the design, the blue solid line $C_y(\bar{\delta})P(\bar{\delta})$ in diagram (a) shows a gain margin of 10 dB or more and a phase margin of 40 degrees or more. It is generally said that the desirable gain margin for a servo system is 10 dB or more and the desirable phase margin is 40 degrees or more. In the dimensionless frequency range below the frequency (bandwidth) at which $G_{ry}(\bar{\delta})$ indicated by the green solid line shows a gain of approx. -3 dB in diagram (b), $S(\bar{\delta})$ indicated by the blue solid line shows low-frequency cutoff characteristics of 60 dB/decade. The control system is thus expected to deliver robustness against disturbances or fluctuations of the controlled object in the low-frequency range.

(7) Verifying the basic design

The steering angle control system in Fig. 14 was modeled on MATLAB®/Simulink® and subjected to simulation by setting $P(\bar{\delta})$ of Eq. (14-1), $Fc(\bar{\delta})$ of Eq. (16-6), $N_c(\bar{\delta})$ and $D_c(\bar{\delta})$ of Eqs. (14-2) and (14-3), and $G_r(\bar{\delta})$ of Eq. (15), as well as parameters of the disturbance generator $G_d(\bar{\delta})$. Transfer Fcn of the Continuous library was used as a transfer function model. Setting the solver to a fixed step ode1 (Euler) and the fixed step size to one (1) allowed computation of a dimensionless discrete time system using the δ operator. Major parameters that were set for the simulation are shown in Table 1.

The results of the simulation are shown in Fig. 17. According to Fig. 17, the control output $y(k)$ follows asymptotically to the target steering angle $r(k)$ that changes in ramp rate until the sampling count k is 500. When a ramp disturbance $d(k)$ is applied at k = 1000, the control output $y(k)$ almost does not change and continues following the target steering angle $r(k)$. No vibration can be found with the steering wheel angle θ_h (k) as well.

Table 1 Major parameter settings for simulation

Parameter	Settings/Description
Target steering angle signal source r_0	1/500 (0 at k = 500)
Disturbance signal source d_0	1/500 (applied at k = 1000)
Disturbance generator	$G_d(\bar{\delta}) = P(\bar{\delta})/(\bar{\delta})^2$
Solver	Fixed step ode1 (Euler)
Fixed step size	1 (dimensionless time)

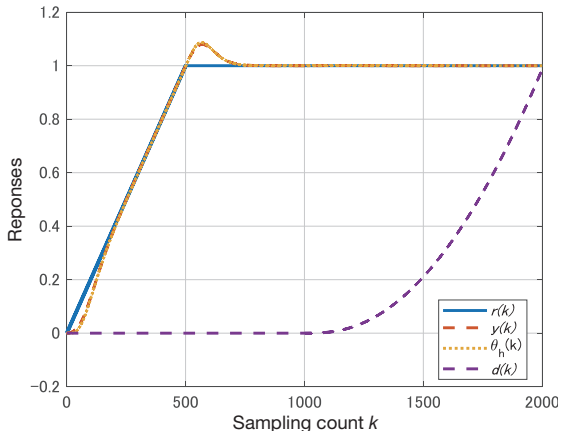

Fig. 17 Results of simulation of steering angle control system

4.3 Detailed Design and Implementation of Compensators

4.3.1 Detailed Design of Compensators

This section describes the detailed design of the compensators. Fig. 18 shows a block diagram of a compensator implementation model. In Fig. 18, the six transfer functions represented by the aforementioned Transfer Fcn are collectively called a "function model" and the transfer function of such a function model implemented in an appropriate way is called an "implementation model" (the term "implement" here refers to expressing a transfer function using state and output equations). For the steering assist control compensator, the pre-compensator in the Figure is $F_c(\delta)$ = 0. In $R(\delta)$, its numerator polynomial parameters depend on the magnitude of the steering assist (assist gain), although a detailed description is omitted here. The area enclosed by the blue broken line in Fig. 18 indicates a block with state variable estimation and feed-

back functions and that enclosed by the red broken line is a block with disturbance estimation and feedback functions. This implies that the parametrization of a stabilizing compensator can be basically applied with the same theory as for compensators using the state variable and disturbance estimation observer [Note 4].

Note 4) An instrument that uses a controlled object model to estimate its state variable and disturbances

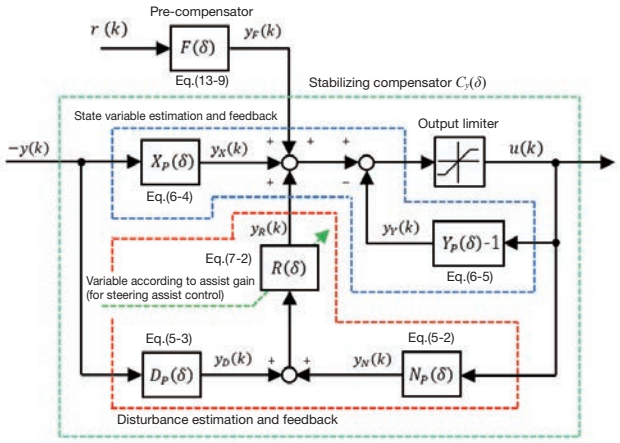

Fig. 18 Block diagram of compensator implementation model

The following introduces an example of implementation of the pre-compensator $F_c(\delta)$. The transfer function of Eq. (13-9) can be expressed as follows:

$$F_C(\delta) = n_F(\delta)/d_F(\delta) + D_F \tag{18-1}$$

where

$$n_F(\delta) = n_{Fn+l-2}\delta^{n+l-2} + \cdots n_{F1}\delta + n_{F0}$$
$$d_F(\delta) = \delta^{n+l-1} + d_{Fn+l-2}\delta^{n+l-2} + \cdots d_{F1}\delta + d_{F0}$$

D_F: constant representing a feedthrough term of $F_C(\delta)$

A possible realization method for lower computation error may be balanced realization (calculation using the MATLAB® function "balreal" for instance). To reduce the computation complexity, we decided to select controllable canonical form (this calculation can also be achieved with the MATLAB® function "canon").

The controllable canonical form of Eq. (18-1) can be expressed by the equation below:

$$\delta x_F(k) = A_F x_F(k) + B_F r(k) \tag{18-2}$$
$$y_F(k) = C_F x_F(k) + D_F r(k) \tag{18-3}$$

where

$$x_F(k) = [x_{F1}(k) \quad x_{F2}(k) \quad \cdots \quad x_{Fn+l-1}(k)]^T$$

$$A_F = \begin{bmatrix} 0 & 1 & 0 & \cdots & 0 \\ 0 & 0 & 1 & \cdots & 0 \\ \vdots & \vdots & \vdots & & \vdots \\ 0 & 0 & 0 & & 1 \\ -d_{F0} & -d_{F1} & -d_{F2} & & -d_{Fn+l-2} \end{bmatrix}$$

$$B_F = \begin{bmatrix} 0 \\ \vdots \\ 0 \\ 1 \end{bmatrix}, \quad C_F = [n_{F0} \quad n_{F1} \quad \cdots \quad n_{Fn+l-2}]$$

Eq. (18-2) can be developed into the equation below:

$$\left.\begin{aligned} x_{F1}(k) &= x_{F1}(k-1) + T_c x_{F2}(k-1) \\ &\vdots \\ x_{Fn+l-2}(k) &= x_{Fn+l-2}(k-1) \\ &\quad + T_c x_{Fn+l-1}(k-1) \\ x_{Fn+l-1}(k) &= x_{Fn+l-1}(k-1) \\ &\quad - T_c\left[\sum_{i=1}^{n+l-1}\{d_{Fi-1}x_{Fi}(k-1)\} + r(k-1)\right] \end{aligned}\right\} \tag{18-4}$$

A compensator implementation model is created on MATLAB®/Simulink® in such a manner that computation is carried out in the order of Eq. (18-4) and Eq. (18-3). For higher model readability, the model creation should be conducted according to the modeling guideline in which the description rule was established based on MAAB [Note 5) 7)].

Note 5) An acronym of MathWorks® Automotive Advisory Board. A guideline that specifies protocols for MathWorks products including description rules.

Compensator computation by microprocessors uses the single precision floating-point format for memory saving. Therefore, control parameters (variables having a fixed value) in Eqs. (18-3) and (18-4) and state variables (whose value changes with time) are all defined with single precision floating-point variables in the implementation model stage.

4.3.2 Verifying the Compensator Implementation Model

The function and implementation models consisting of the six transfer functions in Fig. 18 are each subject to a back-to-back test to verify that these models are equivalent to each other.

4.3.3 Implementing Compensators

As described in section 3.3, Embedded Coder® is used to automatically generate a C code from the implementation model. The generated C code is checked for conformance to the MISRA-C® [Note 6)] rules using a static analysis tool. Any nonconforming items are remedied [7)]. Verification of the implementation results will be described in the next chapter.

Note 6) Coding standards intended to ensure safe, portable, and reliable software (in C-language)

5 Design Verification

This chapter provides an example of the results of verification of the compensator design for steering assist control according to the verification process.

5.1 Compensator Unit Evaluation

Software integrated with a designed compensator was implemented in the power pack. The power pack was then applied with sinusoidal signals as motor current commands. From input and output signals of the compensator, the frequency characteristics of the compensator $C_y(\delta)$ were measured. The results are shown in Fig. 19.

The measurement results closely match the functional model, verifying that the compensator has been implemented as designed. Note that the results shown in Fig. 19 are for another design different from the basic design described in 4.1.5 Example of Basic Design of Compensator.

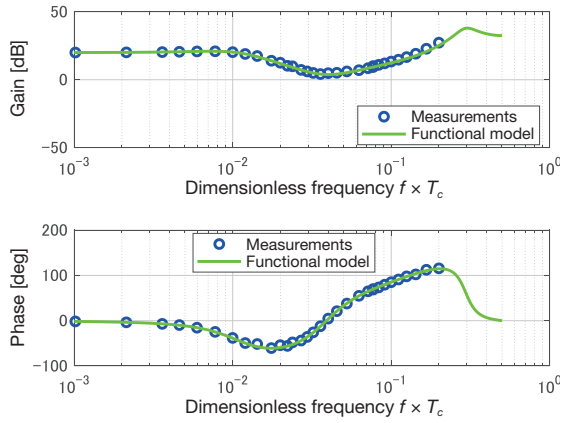

Fig. 19 Example of results of unit evaluation of compensator $C_y(\delta)$

5.2 System Evaluation and Redesigning of Compensators

The system shown in Fig. 8 was applied with sinusoidal waves as motor current commands to measure the frequency characteristics of the controlled object. The frequency characteristics of the controlled object are shown in Fig. 20. The figure plots the frequency characteristics of the compensator design model of Eq. (8-1) (hereinafter the "basic design model"), of the measurement results, and of a model identified from the measurement results.

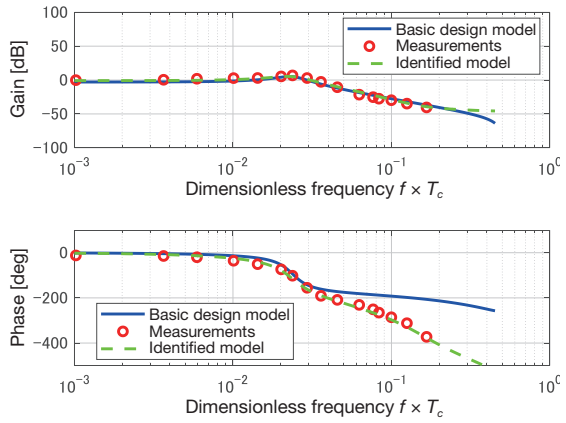

Fig. 20 Frequency characteristics of controlled object

The identified model was obtained by calculating the frequency response vector from the measurement data using the MATLAB® function "fft" and then determined with the MATLAB® function "invfreqz". Transfer function parameters determined with "invfreqz" are written in the z operator form. The obtained parameters were thus converted into the δ operator form. The identified model in Fig. 20 can be expressed by the equation below:

$$P(\bar{\delta}) = \frac{n_P(\bar{\delta})}{d_P(\bar{\delta})} = \frac{n_{P3}\bar{\delta}^3 + n_{P2}\bar{\delta}^2 + n_{P1}\bar{\delta} + n_{P0}}{\bar{\delta}^4 + d_{P3}\bar{\delta}^3 + d_{P2}\bar{\delta}^2 + d_{P1}\bar{\delta} + d_{P0}} \tag{19-1}$$

where

$$n_P(\bar{\delta}) = 5.317\times10^{-3}(\bar{\delta} + 0.1864) \times(\bar{\delta}^2 - 0.2701\bar{\delta} + 1.600)$$
$$d_P(\bar{\delta}) = (\bar{\delta}^2 + 0.5513\bar{\delta} + 8.201\times10^{-2}) \times(\bar{\delta}^2 + 9.755\times10^{-2}\bar{\delta} + 2.135\times10^{-2})$$

All the gains of the basic design model, measurements, and identified model decrease after around a dimensionless frequency of 0.02 at nearly -40 dB/decade, showing relatively good agreement with each other. However, the phase of the measurements is much behind the basic design model after around a dimensionless frequency of 0.03. Possible causes include a response delay of the actual current from the motor current command, the control computation time of the software, frictional torque and small rattling of the machinery, and deflection of the elements that were assumed to be rigid bodies, which were not taken into account in Eq. (8-1).

Since the gain and phase of the measurements are in good agreement with those of the identified model, the controlled object can be approximately expressed in a transfer function of degree 4 as shown in Eq. (19-1).

In fact, the frequency characteristics of the actual controlled object show a larger phase delay than that of the basic design model. This means that a compensator designed based on the basic design model may fail to keep the control system stable. Then, we have redesigned the compensator using the identified model of Eq. (19-1). The redesigned compensator can be expressed by the equation below:

$$C_y(\bar{\delta}) = \frac{n_{NC}(\bar{\delta})}{n_{DC}(\bar{\delta})} \tag{19-2}$$

where

① For large steering assist torque:

$$n_{NC}(\bar{\delta}) = 22.847(\bar{\delta} + 8.494\times10^{-2}) \times(\bar{\delta}^2 + 0.5513\bar{\delta} + 8.201\times10^{-2}) \times(\bar{\delta}^2 + 0.1579\bar{\delta} + 1.889\times10^{-2})$$
$$n_{DC}(\bar{\delta}) = (\bar{\delta} + 0.1864)(\bar{\delta} + 3.666\times10^{-2})^2 \times(\bar{\delta}^2 + 1.295\bar{\delta} + 0.7986)$$

② For middle steering assist torque:

$$n_{NC}(\bar{\delta}) = 18.246(\bar{\delta} + 0.1022) \times(\bar{\delta}^2 + 0.5513\bar{\delta} + 8.201\times10^{-2}) \times(\bar{\delta}^2 + 0.1646\bar{\delta} + 1.701\times10^{-2})$$
$$n_{DC}(\bar{\delta}) = (\bar{\delta} + 0.1864)(\bar{\delta} + 6.502\times10^{-2})^2 \times(\bar{\delta}^2 + 1.262\bar{\delta} + 0.7211)$$

③ For small steering assist torque:

$$n_{NC}(\bar{\delta}) = 12.111(\bar{\delta} + 0.1336) \times(\bar{\delta}^2 + 0.1745\bar{\delta} + 1.250\times10^{-2})$$

$$\times(\bar{\delta}^2+0.5513\bar{\delta}+8.201\times10^{-2})$$
$$n_{DC}(\bar{\delta})=(\bar{\delta}+0.1864)(\bar{\delta}+0.1127)^2$$
$$\times(\bar{\delta}^2+1.200\bar{\delta}+0.6005)$$

$1/f(\delta)$ in Eqs. (5-2) and (5-3) is the matched pole-zero model of the following stable transfer function $1/f(s)$ that has been made dimensionless with the control frequency $1/T_c$:

$$1/f(s)=1/\ \{f_1(s)f_2(s)\} \tag{19-3}$$

where

$$f_1(s)=s^2+2\zeta_{f1}\omega_{f1}s+{\omega_{f1}}^2$$
$$f_2(s)=s^2+2\zeta_{f2}\omega_{f1}s+{\omega_{f2}}^2$$
$$0<\omega_{f1},\quad 0<\omega_{f2},\quad 0<\zeta_{f1},\quad 0<\zeta_{f2}$$

where $\zeta_{f1}=\zeta_{f2}=1$ and $\omega_{f1}=\omega_{f2}=2\sqrt{K_{pe}/I_{pe}}$. $1/g(\bar{\delta})$ in Eqs. (6-4) and (6-5) is the matched pole-zero model of the following stable transfer function $1/g(s)$ that has been made dimensionless with the control frequency $1/T_c$:

$$1/g(s)=1/\ \{g_1(s)g_2(s)\} \tag{19-4}$$

where

$$g_1(s)=s+\omega_{g1},\quad g_2(s)=s^2+2\zeta_{g2}\omega_{g1}s+{\omega_{g2}}^2$$

where $\zeta_{g2}=1$, $\omega_{g1}=\omega_{g2}=2\sqrt{K_{TB}/I_{pe}}$.

Next, the parameter for the pole $1/d_d(\bar{\delta})$ of the disturbance model of Eq. (9-1) was set as follows:

$\omega_d=0.5\sqrt{K_{pe}/I_{pe}}$: Large steering assist torque

$\omega_d=0.9\sqrt{K_{pe}/I_{pe}}$: Medium steering assist torque

$\omega_d=1.5\sqrt{K_{pe}/I_{pe}}$: Small steering assist torque

In all these cases, $\zeta_d=1$.

Also, it is assumed that the pole of the free parameter $R(\bar{\delta})$ in Eq. (9-3) is the matched pole-zero model of $1/g_1(s)$ stated above.

The frequency characteristics of the redesigned $C_y(\delta)$, $C_y(\delta)P(\delta)$ (loop transfer function), and $S(\delta)$ are shown in Fig. 21. As a result, the gain margin is 5 dB or more and the phase margin is 30 degrees or more in all cases. It has been verified through system evaluation and actual vehicle evaluation that a stable control system has been obtained with the redesigned compensator, although a detailed description is omitted here.

5.3 Actual Vehicle Evaluation

In in-house actual vehicle evaluation, a vehicle of an existing model is used to mainly test stationary steering (steering of a stopped vehicle). The test driver should start to turn the steering wheel and then turn it back to check the effect of the steering assist. The driver should also check that they feel no vibration via the wheel. The tuning parameters include the parameters of Eqs. (19-3) and (19-4), the parameters of the pole of the disturbance model of Eq. (9-1), and the parameters of the poles of Eq. (9-3). In in-house actual vehicle evaluation, several compensator candidates of different designs should be prepared by modifying the tuning parameters stated above toward actual vehicle evaluation at customer sites.

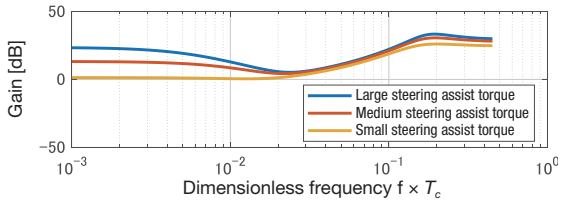

(a) Frequency characteristics of compensator Cy(δ)

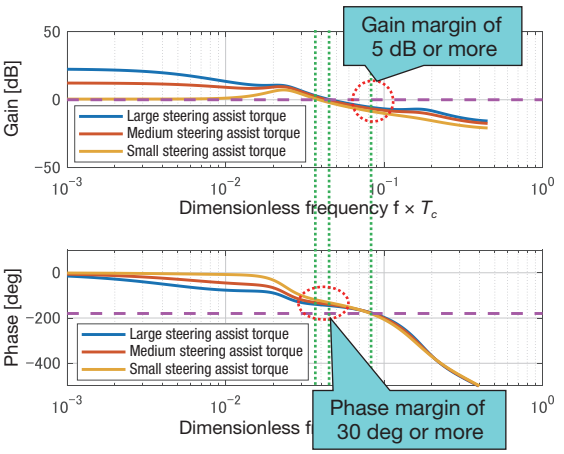

(b) Frequency characteristics of loop transfer function Cy(δ)P(δ)

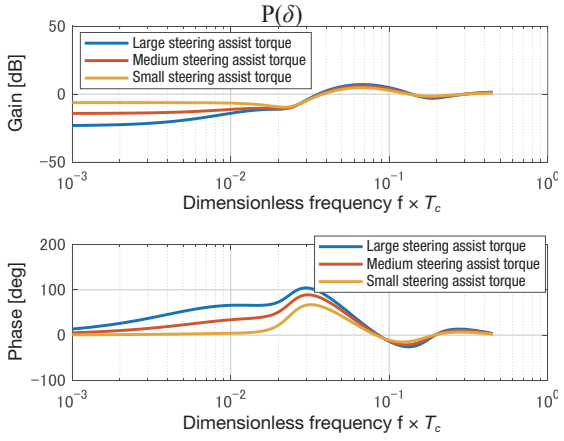

(c) Frequency characteristics of transfer function $S(\delta)$

Fig. 21 Frequency characteristics of redesigned steering assist control system

In actual vehicle evaluation at customer sites, a driving test is carried out on a dedicated off-road test course, in addition to the stationary steering evaluation. During the driving test, particularly the driver's feeling of steering at the start of cornering and of kickback during driving straight ahead or cornering should be checked.

6 Future Outlook

The approach explained in this report is just a compensator design method applicable to existing EPS that is a little bit different from the traditional approach. The importance of electronically-controlled in-vehicle equipment will rise as in-vehicle equipment automation and autonomous driving is further accelerated. As an in-vehicle equipment manufacturer, KYB needs to develop various value-added products. In the course of the development, not only electrical and machine element engineers but also control technology engineers should play two major roles of:

① crystallizing and screening product ideas during the product planning stage to create new products, and;
② developing a robust design to minimize uncertainty throughout the product lifecycle.

For role ①, just think about sensors, for instance. What are the minimum sensors that can deliver the functions and control performance required by the product (for cost reduction)? What physical amounts should be detected and controlled to satisfy the requirements (for higher added-value)? An effective means to solve these possible challenges is to identify controllability and observability of the system from the control technology perspective and to utilize the observer theory. For role ②, a parametric model involving uncertainty may be identified through simulation using a model with product quality (production variations) and secular changes in quality taken into account or through their testing on an actual machine. Such a parametric model can be effectively used to design compensators, ensuring robust stability of the control system.

Based on the above, we would like to strengthen our product design and proposal capabilities.

7 Concluding Remarks

Focusing on EPS for all-terrain and utility task vehicles, this report explains KYB's control technologies for in-vehicle electric actuators by introducing some numeric examples. The basis of the technologies is a design approach based on parametrization of stabilizing compensators, which has been developed into a discrete time system in the δ operator form. The various equations used for compensator calculation were converted into software programs with m-file [Note 7)]. This allows automatic calculation of parameters for the function and implementation models of compensators just by setting the tuning parameters described in Section 5.3.

Note 7) A text file that describes programs to be executed on MATLAB®

The control technologies explained in this report can be applied not only to electric actuators but also to electric pumps, hydraulic actuators, and other various electronically-controlled components.

Although compensators only make up a small proportion of in-vehicle software-controlled components, they are an essential technology directly affecting security, safety, and comfort. We would like to continue contributing to the improvement of quality and added-value of KYB products with our system analysis and evaluation techniques, control technologies, and software technologies.

Finally, we would like to take this opportunity to sincerely thank all those concerned who have extended guidance and cooperation to us in implementing and evaluating these control technologies.

References

1) MIYAKE, TOMITA: Development of EPS for Non-Passenger Vehicles, KYB Technical Review No.60, pp 60-63, (2020).
2) INAMITSU, HORI: Development of Active Suspension by KYB, KYB Technical Review No.63, pp 9-14, (2021).
3) MAEDA, SUGIE: System Control Theory for Advanced Control, Asakura Publishing, (1990).
4) ADACHI: System Identification Theory for Users, The Society of Instrument and Control Engineers, (1993).
5) KANAI, HORI: An Introduction to Digital Control System -Application of Delta Operator-, Maki Shoten, (1992).
6) KITAMURA: Development of Simulation Technology for EPS System, KYB Technical Review No.59, pp 17-24, (2019).
7) KOBAYASHI: Application of MBD to Development of ECU Prototype for EPS, KYB Technical Review No.52, pp 49-53, (2016).

Author

MATSUMOTO Daisuke

Joined the company in 1995.
Development Sect. No.2, Electronics Technology Dept., Engineering Headquarters, Automotive Components Operations
Special Sect. Manager, Basic Technology R&D Center, Engineering Div.
Engaged in analysis of in-vehicle actuators and development of their controls

ENOMOTO Daisuke

Joined the company in 2018.
Development Sect. No.2, Electronics Technology Dept., Engineering Headquarters, Automotive Components Operations
Engaged in analysis of in-vehicle actuators and development of their controls

KENJYO Kazunori

Joined the company in 2015.
Chief Researcher, Electronics Technology Sect., Basic Technology R&D Center, Engineering Div.
Engaged in research and development of control software for in-vehicle actuators

FUKUSHI Natsuru

Joined the company in 2017.
Chief Researcher, Electronics Technology Sect., Basic Technology R&D Center, Engineering Div.
Engaged in research and development of control software for in-vehicle actuators

Product Introduction

Development of Vane Pump for Medium Passenger Vehicle CVT

HAGIWARA Takahiro, OOTAKI Masashi, KONDO Hirotoshi, SHINDO Shota

1 Introduction

This report introduces a vane pump for medium passenger vehicle CVT Note 1). This vane pump will be mounted, as a hydraulic power source, to the transmission mechanism for medium passenger vehicles developed by JATCO Ltd. as the successor of existing CVT unit that has already been in mass production and rolled out globally.

Production of this product was started at KYB Kanayama in October 2020.

Note 1) An acronym for Continuously Variable Transmission.

2 Newly Developed CVT Unit

Compared with the existing type, the new CVT unit that has just been developed by JATCO Ltd. has the following features:

① Lower fuel consumption due to lower friction
② Superior operation feeling
③ Lower NVH Note 2)

The new CVT unit has been developed on the assumption that it will mainly be combined with an environmentally friendly downsized turbo engine.

The product is backed up by a global supply chain with production sites including Japan, China, and Mexico.

Note 2) An acronym for Noise, Vibration, and Harshness.

Photo 1 Appearance of new CVT unit
(Extracted from JATCO Ltd.'s website)

3 Newly Developed Vane Pump

Partly because it was to be mounted as the successor of the existing CVT, the new vane pump needed to be rolled out globally including Japan, China, and Mexico in the same manner as for the existing vane pump. So, it was mandatory to achieve a sophisticated design quality during the development stage.

Based on the existing vane pump, we promoted the development of a new model with a focus on the discharge performance and durability being equivalent to or superior to that of the existing model as well as lower friction. As a trade-off for lower friction with equivalent discharge performance, a vane pump will inevitably be less durable. Still, we obtained an optimal design satisfying the specification requirements.

Furthermore, we strove to reduce the pump weight for environmental conservation and lower the production cost that was also demanded by end-users.

Photo 2 shows the appearance of the newly developed vane pump. Table 1 shows the detailed specifications and Table 2 the major improvements.

Photo 2 Appearance of new vane pump

Table 1 Specifications of new vane pump

Type	Balanced vane pump
Basic discharge	11.3 cm^3/rev
Pump revolutions	Up to 7300 rpm
Discharge pressure	Up to 6 MPa
Oil temperature	-40°C - 140°C
Production site	Japan, China, Mexico

Table 2 Performance improvements

Improvements	・A notch in the cam ring ・Aluminum cover instead of iron cover ・Ports of an optimal shape

4 Performance Improvements

4.1 Optimally Designed Cam Ring Notch

To ensure that the CVT unit can deliver lower friction for lower fuel consumption, the driving torque of the vane pump must be reduced.

The driving torque equation for vane pumps can be expressed as (Basic discharge × Pressure) / 2π. Since there is no change in service pressure between the existing and new models, the basic discharge was reduced for lower driving torque. However, a precondition was that the new model must meet the performance specifications equivalent to those of the existing one.

The new vane pump is of a type with an integral flow control valve (spool). It should be designed to internally maintain a flow rate that can well cover the required discharge characteristics according to the pump speed.

A vane pump with an internal flow control valve can make use of the power of any excessive internal circulating flow to enhance the suction capability (Fig. 1).

In designing the new pump, the basic discharge was reduced, resulting in about 10% lower internal circulating flow. This led to lower suction capability, making the pump likely to suffer cavitation (Fig. 2).

Cavitation is a phenomenon in which the air dissolved in the hydraulic fluid forms bubbles. Repetitive formation and collapse of such bubbles wears and damages the pump components. This is because we expected the new vane pump to be unable to satisfy the requirements for durability testing merely by reducing the basic discharge while keeping the other specification items unchanged from the existing ones.

Several countermeasures could be considered. From the viewpoint of cost-effectiveness, we introduced a "notch" in the suction part of the cam ring that serves as a suction oil path. The notch expanded the suction oil path to reduce the pressure loss, raising the suction capability (Fig. 3).

In response to the introduction of the notch, the surface pressure on the cam ring applied by the sliding vanes increased, resulting in a higher PV factor Note 3). This resulted in various durability disadvantages including abnormal wear of the cam ring.

Then, in order to determine the balance between the notch depth and the PV factor, in other words, the point at which performance and durability can go hand in hand, the new vane pump was subjected to a durability test to identify the critical point. We finally determined the optimal size of the notch (Fig. 4).

Through these development efforts, the new vane pump satisfied both the durability and performance requirements, achieving the lower driving torque as aimed for.

Note 3) PV factor = P (surface pressure) × V (velocity); One of the wear factors

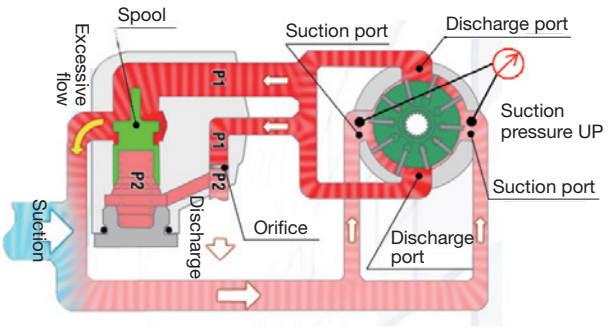

Fig. 1 Oil circulation in vane pump

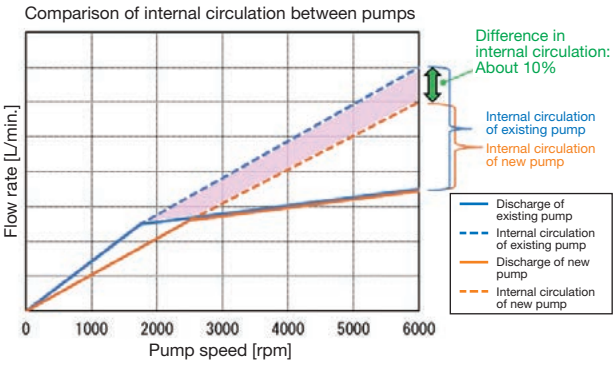

Fig. 2 Comparison of internal circulation between pumps

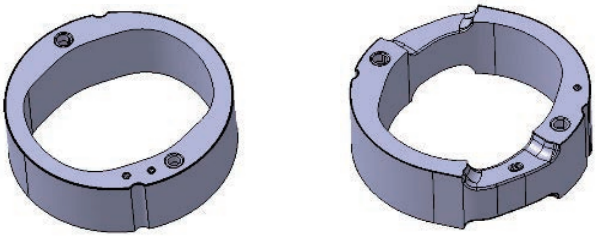

Fig. 3 Comparison of cam ring specifications

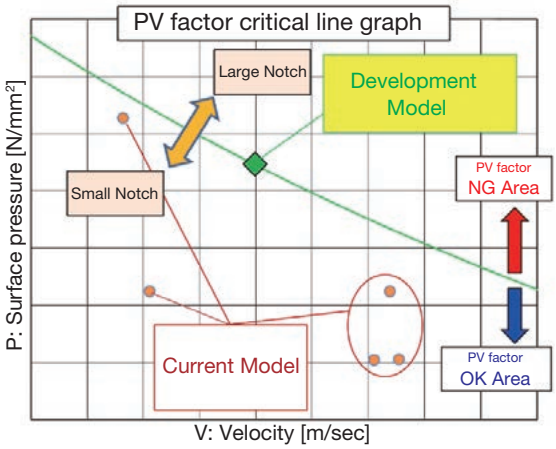

Fig. 4 PV factor critical line graph

4.2 Aluminum Cover Instead of Iron Cover (Weight and Cost Reduction)

The existing vane pump for medium passenger vehicle CVT used a core oil path cover made of cast iron (Figs. 5 and 6). The new product has been designed to have an aluminum diecast cover. With this design, the weight of the cover alone has been reduced by 350 g, which is an approximately 30% reduction in the total weight of the vane pump, contributing to substantial weight reduction, and consequently lower fuel consumption.

Furthermore, the manufacturing method has been changed from the cast iron system to an aluminum diecast system. This has helped improve the productivity and reduce the manufacturing cost.

Along with the introduction of the aluminum diecast cover, however, the geometry of the oil path inside the cover changed in such a manner that the oil was unlikely to flow smoothly. We noticed that the new oil path geometry worsened the pump's NVH (Figs. 7 and 8).

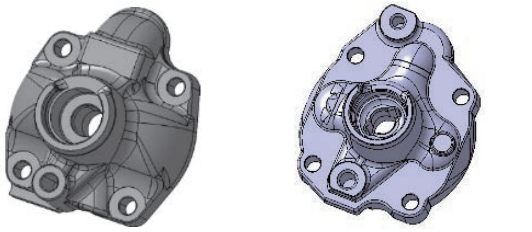

Existing (cast iron) New (aluminum diecast)

Fig. 5 Comparison of appearance of cover

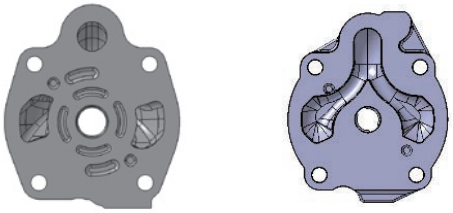

Existing (core oil path) New (diecast oil path)

Fig. 6 Comparison of oil path

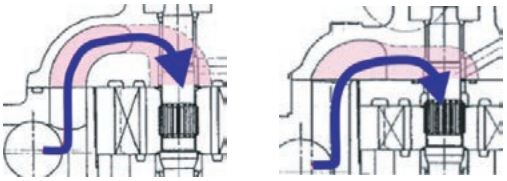

Existing (core oil path) New (diecast oil path)

Fig. 7 Comparison of flow in oil path

Existing (core oil path) New (diecast oil path)

Fig. 8 Visual comparison of pressure loss in oil path

4.3 Ports of Optimal Shape

It was mandatory to improve the pump's NVH in order to satisfy the requirement that the NVH of the new pump be equivalent or superior to that of the existing model. However, the oil path of the new cover, which was a factor that deteriorated NVH, could not be improved from the viewpoint of manufacturing method. It was impossible to design an oil path for the diecast cover that is similar to that of the cast iron cover.

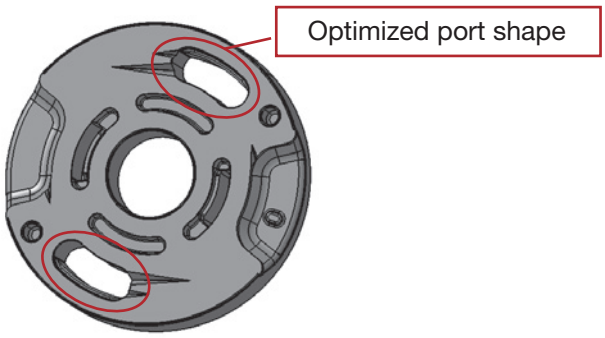

Fig. 9 Ports of side plate

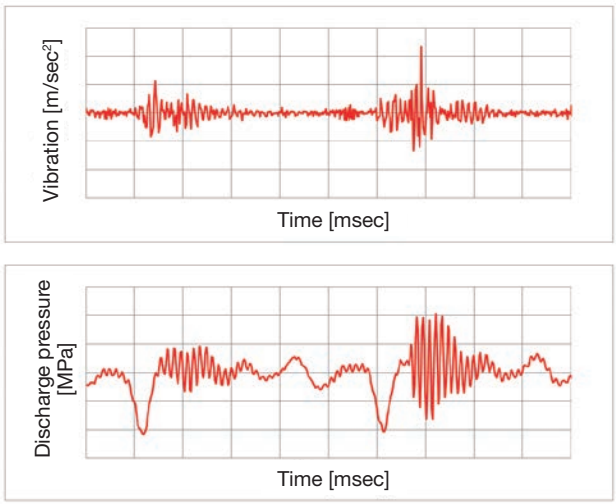

Fig. 10 Pump discharge pressure and vibration before improvement

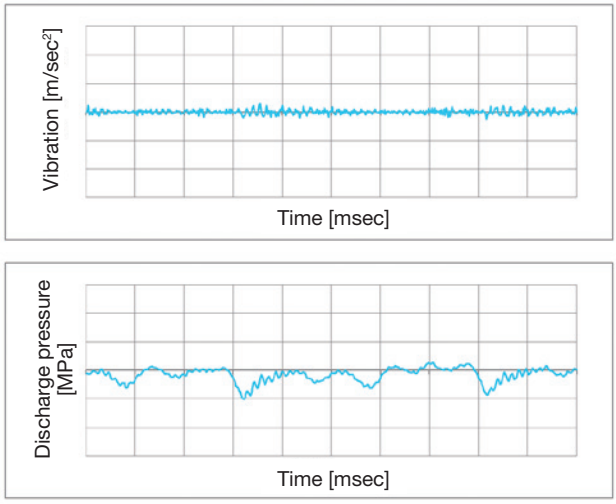

Fig. 11 Pump discharge pressure and vibration after improvement

Then, we decided to pursue an optimal shape of the ports of the side plate for the aluminum cover. With the optimal port design, the discharge pulsation was reduced to suppress the vibration, satisfying the NVH requirement (Figs. 9, 10 and 11).

5 Evaluation

This development project was highly rated by JATCO Ltd. and won the FY2020 JATCO QCDS Best Performance Award.

This prize is awarded only to the one company globally rated as overall No.1 in development, quality, cost and delivery. We were only able to win this prize with the cooperation from those concerned not only in Development but also in other departments. We would like to take this opportunity to deeply thank all those concerned.

As a quality-specific prize, we also won the JATCO Regional Special Award at the same time.

Furthermore, KIMZ (KYB Industrial Machinery (Zhenjiang)), which launched production in March 2021 after KYB Kanayama was established, won the QCDS A-rank Award. KYB has been highly evaluated both at home and abroad.

Photo 3 QCDS Best Performance Award (right), Regional Special Award (left)

Photo 4 QCDS A-rank Award (China)

6 Conclusions

Compared with the existing model, this newly developed product has achieved the following:

① About 10% lower pump driving torque
② About 30% lighter pump
③ Simultaneous achievement of durability and low driving torque
④ Lower noise
⑤ Lower cost

The considerations discussed in this development project are shown in the inclined developed views of the existing and new products (Fig. 12).

7 In Closing

We sincerely appreciate the cooperation of all those engaged in program development from JATCO Ltd. and all other partner companies and all those concerned in relevant KYB departments.

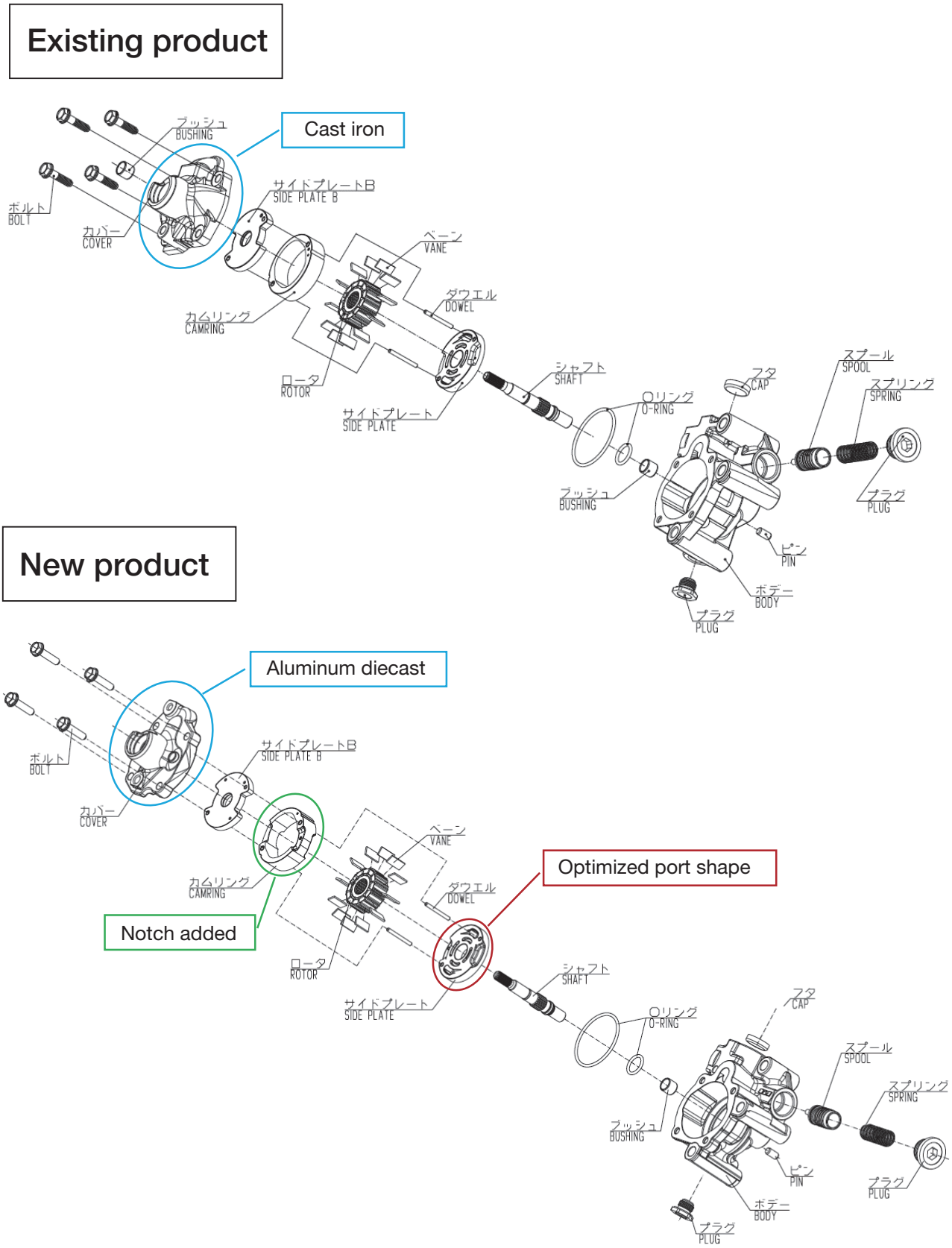

Fig. 12 Inclined developed views of existing and new products

Author

HAGIWARA Takahiro

Joined the company in 2010.
Pump Engineering Dept., Steering Business Dept., Automotive Components Operations
Engaged in design of vane pumps.

OOTAKI Masashi

Joined the company in 2012.
Pump Engineering Dept., Steering Business Dept., Automotive Components Operations
Engaged in design of vane pumps.

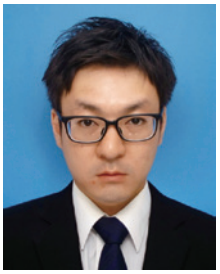

KONDO Hirotoshi

Joined the company in 2013.
Gifu Local Office, Basic Technology R&D Center, Engineering Div.
Engaged in design of vane pumps.

SHINDO Shota

Joined the company in 2014.
Pump Engineering Dept., Steering Business Dept., Automotive Components Operations
Engaged in design of vane pumps.

Essay

Essay from Expatriate at HKE

HATTORI Koji

1. Introduction

KYB launched a joint-venture project with the Henglong Group of China in August 2017. The project was implemented under the company's policy to shift the business base of electric power steering (EPS) for passenger vehicles from Japan to China.

Before that, KYB had surveyed parts suppliers in China as part of its cost reduction activity for EPS parts. The Henglong Group was among those with whom KYB had already gotten in touch. However, a joint-venture relationship is quite different from a business partnership in scale and relevance. I remember that I recognized the launch of the project as a big milestone.

I am, and was at that time too, in charge of cost planning. I was involved in the joint-venture project to study the commercial feasibility of the project from the cost perspective. Actually, I was quite frustrated about the limited information we could obtain from the other party because cost information is very sensitive until both parties enter into a formal joint-venture contract.

In April 2018, the joint-venture contract was concluded and Hubei Henglong & KYB Automobile Electric Steering System Co., Ltd. (hereinafter "HKE") was formally established. To set up a cost planning organization for the first time for the Henglong Group, I was assigned to work for HKE in China, which was my second expatriation following the first one to the U.S. in 2005. I moved to China with five colleagues of mine at the end of November 2018.

Photo 1 Appearance of HKE building

2. Jingzhou City, Hubei Province

HKE is located in Jingzhou City, Hubei Province in China. Jingzhou is about 200 km inland and west of Wuhan in the same province, which is considered to be the origin of COVID-19 that continues to severely affect the world today. Compared to Japan, Jingzhou City is located at a latitude south of Tanegashima, which may give you the impression that Jingzhou is a tropical place. However, the climate there is very similar to that of Kani City, Gifu Prefecture in Japan where Gifu North Plant is located. While in the summer it is so hot and humid in Jingzhou that the temperature rises to 35°C or more for consecutive days, it sometimes snows in the winter.

At the end of 2018, in the month after I was sent to Jingzhou, several centimeters of snow fell. I heard that snow accumulation was quite rare in recent years. Small children were playing in a lively way with the snow in the courtyard of the apartment where I lived. That was my first experience to spend the year-end period in China and I felt happy to see scenery similar to that in Japan.

Photo 2 Snow at the end of 2018

Jingzhou City occupies an area of 14,067 square kilometers. Spreading along the meandering Yangtze River, the entire city is rich in water with a network of distributary channels, waterways, and lakes. Many beaches and parks located along the Yangtze River are occupied by families and couples enjoying holidays. With this geographical advantage, Jingzhou City is an important site of maritime transportation and physical

distribution in the middle reaches of the Yangtze River. Historically, the city is famous for its strategically important location as seen in the Romance of the Three Kingdoms. A gigantic statue of Guan Yu (total height of 58 meters), who was a bold military general assigned to govern Jingzhou, had previously existed as a symbol of the city. Unfortunately, it became evident just before my repatriation that the statue was an unlawful construction and it has now already been demolished. (I heard that there was a plan to relocate the statue, but no relocation work seems to have been carried out at this moment).

Photo 3 Now-lost world's largest statue of Guan Yu

3. Working in HKE

As mentioned above, my duties during the stay in Jingzhou City were to kick off the cost planning operation for the first time for the Henglong Group and to proliferate the visualization and standardization of cost issues, in order to achieve a suitable product cost and EPS business profitability. However, it was quite difficult for me to get the Chinese staff to understand the operation as it was their first job of this kind. I prepared a cost planning manual and related documents on the operation in PowerPoint and translated the text into Chinese. After distributing the documents and holding seminars, I received my first request from the staff. They asked me to do a job, saying "we want to buy some curtains for the office, please do a cost assessment".

While I encountered various "difficult-to-understand" events like this, I built a friendship with my Chinese colleagues through monthly dinners and birthday parties within the department. Meanwhile, the project gradually got on track, enabling us to carry out cost reduction activities and build a collaborative relationship with related departments in a manner similar to how we did in Japan. Then, worrying news came as we approached the end of 2019.

Photo 4 Shore of Yangtze River with many families enjoying a holiday

4. Terrible Shock

There were rumors that a new type of pneumonia had emerged in a seafood market in Wuhan City, which is near Jingzhou City. This was the later-named COVID-19 as I mentioned above.

The seafood market deals with not only seafood but also all kinds of foodstuffs. I even heard a Chinese saying expressing the richness of the food culture that "we eat everything with four legs except tables and everything that flies except airplanes". It is regular practice to even treat some wild animals as food, many of which may look unacceptable to the Japanese. Since COVID-19 was said to originate in such wild animals, Chinese people around me were rather optimistic at the beginning. When I visited a local supplier, people there said "it is OK because the seafood market has been closed" or "COVID-19 does not involve human-to-human transmission". Television news generally reported similar stories. While I was wondering if things were really so positive, I never ever imagined at that time that such a terrible situation would actually occur.

The first time COVID-19 affected me was during the Chinese New Year holidays. Based on the lunar calendar, the Chinese New Year vacation in 2020 began on January 23, which was earlier than most years. During the vacation, I tried to temporarily go back to Japan and found a dramatic change in circumstances. All flights scheduled to arrive at Wuhan Airport were reportedly going to be canceled in the morning of the day I went to the airport. Among the Japanese expatriates, half were supposed to fly back to Japan on another flight the next day for the sake of air ticket arrangement. We were very anxious whether the flight would take off as scheduled. In the end, the flight on the next day was the last one to Japan before Wuhan Airport was fully closed. All the expatriates in HKE successfully returned to Japan safely. Unfortunately, many expatriates of Japan -based corporations were left out in Wuhan. The news that they were eventually transported to Japan by a government-chartered flight is still fresh in my memory.

Although we managed to come back home safely, we could not return to China even after the lunar New Year vacation was over due to the large-scale city lockdown by the Chinese government. In the end, we continued working online with China for eight months altogether. In addition to the time-zone difference of one hour between Japan and China, which might not be so large, there is a language barrier. Under these circumstances,

doing remote work without face-to-face communication unfortunately affected the human relationship between us that had been built with our relentless efforts. This is a sad memory.

After an eight-month stay in Japan, I was finally permitted to return to China. Still, the immigration restriction, which persists even now, was very strict. Firstly, we were required to take a PCR test at the airport when we arrived to prove we were negative for COVID-19. We were quarantined in a hotel room near the airport for two weeks. We were required to take two further PCR tests during the quarantine period. Then, we went back to Jingzhou and took another PCR test. After returning to the apartment that we lived in, we had to quarantine for another two weeks. Upon completion of the quarantine, we had to take yet another PCR test. By the way, I had had a PCR test before I left Japan to begin with. That was six PCR tests in one month, which were needed for me to enter China. The Chinese government raised their guard against foreigners coming in from abroad, while those who had never taken a PCR test at all were still walking around in the city as usual. I could not help thinking who was the more dangerous.

Photo 5 Wuhan Airport where I arrived in September 2020

5. Living in China

I'm afraid I have told a somewhat cheerless story overall, so I would now like to tell you a little bit happier story for those who will be future expatriates. The word "China" may first remind you of historical culture and cuisine. For your information, the Japanese often say that China has four thousand years of history, but I have heard that the Chinese prefer to say that China has five thousand years of history. When you talk about history with Chinese people, be careful not to say, "four thousand years of history", which may cause them to doubt this phrase.

Unfortunately, I had little chance of enjoying travelling during my assignment in China due to COVID-19. Before the COVID-19 pandemic, I had the opportunity of visiting the Great Wall, which may be the first thing that comes to mind for the Japanese when talking about famous historic buildings in China. As is usual for other similar buildings or great natural sites throughout the world, the Great Wall also has been arranged as a typical sightseeing venue or amusement spot. Still, the gigantic, overwhelming structure in the land was so impactful that it moved me a lot when I saw it with my own eyes. That was a wonderful experience for me. Because it is recognized throughout the world, I intentionally visited the Great Wall on a day outside the busy period, but the site was still so crowded that I found an area around a hilltop along the course of the Wall fully covered by people and could not see the architecture.

Photo 6 The Great Wall crowded with visitors

Speaking of food, Jingzhou cuisine includes many spicy dishes partly because of its closeness to Sichuan Province and Chongqing. People who like spicy food can enjoy many varieties of local delicious cuisine. I actually got hooked on pork intestine (or "fei chang" in Chinese). This so-called "hormone" in Japan can be eaten in China in various ways including as a pot dish and ramen. Fried fei chang with a good amount of hot red pepper was particularly marvelous. I loved its spicy taste and texture that perfectly matched the rather weak Chinese beer of low alcohol content. I frequently used to go to one good restaurant even alone after it had been introduced to me. With many other family customers in the restaurant, a Japanese who could hardly speak Chinese had taken the trouble to come there alone to eat typical local food. I

Photo 7 Fried fei chang

wonder if I looked rather strange to the other customers. Even among the Chinese, some like fei chang but some others do not because of its unique taste. Those who like it sometimes asked me to go out to enjoy fei chang together as we developed a sense of collegiality. That made me recognize that Chinese culture values eating more than is the case in Japan.

6. Farewell

Bearing in mind that I would appoint a Chinese employee to be my successor, I selected and trained local employees after becoming an expatriate in HKE. Today, one of my subordinates at the time has taken over my activities. My colleagues with whom I became good friends still keep in touch with me in public and private life. I consider it a lifelong achievement for me to have established these relationships.

After much joy and hardship, I was directed by the company to repatriate in January 2022 after the first term of the HKE joint-venture contract was to finish. I regretted that there were still many things I had not yet done, but HKE successfully ended the fiscal year 2021 in the black for the first time since its foundation, which was a milestone for me before returning home. It was very emotional for me to be able to say a joyous goodbye to the colleagues with whom I had earlier struggled.

Photo 8 My colleagues at HKE Finance/Cost Planning with whom I worked

7. In Closing

Among my Japanese colleagues who were sent to HKE together in 2018, some are still working hard there even without a temporary return to Japan under the Chinese government's zero-corona policy with no end in sight. Because of its geography, Jingzhou is an inland center for peripheral ethnic minorities and seldom accessed by Japanese, so they are working and living in a very different environment and having to deal with stress. They are making efforts to develop profitable products by putting the EPS business on track under this stress. Hoping that they will be able to proudly return to Japan in the near future, I would like to close this report.

Finally, I would like to express my appreciation to those who extended support and cooperation to me during my assignment in HKE and sincerely hope that HKE and its EPS business will further develop in future.

Author

HATTORI Koji

Joined the company in 1989.
Expatriate in KYB Asia Pacific Corp. Ltd.
Took present post after working in Steering Design Dept., expatriate in the U.S. (Detroit), working in Product Planning Dept., working in PS Cost Planning Dept., and as an expatriate in China (HKE).

Essay

Essay from Expatriate at KMEX

KAWAI Hiroshi

1. Introduction

I was assigned to work for KYB Mexico S.A. de C.V. (hereinafter "KMEXDF") from May 2015 to April 2022. KMEXDF is a sales center of commercially available SA (shock absorbers) for the Mexican market as well as for all other Latin American countries (except Brazil).

I have long been involved with Mexico personally as well. My involvement with the country began with travelling as a backpacker in my schooldays, followed by another experience as an expatriate there. These experiences are linked to this assignment at KMEXDF, further leading to my current position. You never know where you have a chance or a turning point in your life.

Through my residence in Mexico for seven years, my soul and body have been completely Mexicanized. I had very valuable experiences in my public and private life, some of which will be introduced in the following:

2. Living in Mexico

Mexico (United Mexican States) is a huge country of united states located between North America and Latin America. The country has a population of 130 million (almost equivalent to that of Japan) and a total area of 1.96 million square kilometers (five times that of Japan). Mexico City, where I stayed as an expatriate, is located almost at the center of the country and has a population of about 21.58 million (1.5 times that of Tokyo) and an area of 1,479 square kilometers (in contrast only around 70% of that of Tokyo). These figures can easily make you imagine that Mexico City is a densely populated, commercially important place.

Mexico City is located on a highland at an altitude of about 2,300 meters. In contrast to the typical image that Mexico is a very hot country, Mexico City has a comfortable climate with an annual mean temperature of 25°C and low humidity which makes life easy, similar to the spring or autumn seasons in Japan.

Mexico has the geographical advantage of linking North America with Latin America and has a very youthful workforce with an average age of 29. From these reasons, many foreign-owned companies, including Japanese ones, have branched out into Mexico, along with their own cuisine and culture from all over the world. It is one of the attractions of the country to be able to experience such a variety of food and culture in this city.

Mexican people are generous, kind, and cheerful. With the amigo spirit, they are very friendly and welcoming of foreigners.

I have talked only about the good things about living in Mexico so far, but I have to point out the issues of traffic jams and security which gave me such a hard time.

A major cause for concern was traffic jams (Photo 1). The public transport in Mexico is where many incidents of pickpocketing or robbery may occur. During my stay in the city, I basically moved by car. It was a 15-minute walk from my home to the office, but in the mornings and evenings it often took nearly one hour to drive there.

Photo 1 Traffic jam during rush hour

As pointed out by a previous expatriate, it is very easy to obtain a driver's license in Mexico because there is no examination system. The traffic is always exceeding the capacity of the roads. Jams occurring somewhere in the city will cause gridlock in the entire city partly because there are numerous complex roads and many one-way traffic streets.

The maintenance of vehicles depends on their owners, although they have to pass the national inspection more or less. On the road, you can always find faulty cars stuck with their hood open as often seen in a movie. This is one of the major causes of traffic jams.

Naturally, roadways cannot bear such heavy traffic, resulting in road surfaces with potholes and deteriorated pavement here and there. This convinced me that the country had a high demand for shock absorber replacement.

I carried out marketing activity while directly experiencing this situation.

Security is another issue as you know. I had a hard time initially during my residence there. Until you are familiar with the local circumstances to some extent, you need to deliberately search for safe places and safe time frames before being able to go out freely.

3. Working in Mexico

I was in charge of purchasing for the initial three years of my assignment. KMEX sells inventory to the Mexican market and deals with a commercial flow called drop shipment (trilateral distribution in which products are directly delivered from plants to customers and billing is made by KMEX) for the Latin American market.

While "purchasing" may sound rather easy, our purchasing operation actually covered a wide range of jobs. I was engaged in a variety of jobs, from placing orders for commercially available SA, following-up the delivery date with suppliers, ensuring proper inventory management, and taking measures for improved order fulfillment, to developing new markets. I initially faced an uphill battle in accomplishing these jobs for which I had little prior experience.

I had to estimate demand and determine the amount of orders while striking a balance between inventories and order fulfilment. To accomplish this job, it is indispensable to monitor the target markets by collecting information from customers and internal sales personnel and to acquire information from and work together with plants and other departments.

In fact, many delays in delivery occurred, not only due to poor demand estimation and other internal factors attributable to KYB, but also due to the global situation and various other external factors specific to the country. These included demonstrations by longshoremen's unions and other labor unions as well as robbery and burglary. As purchasing manager, I was often called upon by and received complaints from customers about inventory runout.

Still, in the course of such complaints and advice given by customers, I was able to listen to voices in the markets and seriously respond to customer demands. It was a great achievement for me to have learned a lot of things and built trustworthy relationships with them.

Besides this, there were various events and topics that affected me during my stay in Mexico. They included the U.S. government's immigration and trade policies to Mexico launched upon inauguration of the new U.S. President in 2016, a big drop in Mexican peso, and COVID-19 issues. Still, Mexico endured the COVID-19 pandemic without suspending activities of its major industries, which allowed KYB to steadily drive sales promotion.

During the assignment, I also took part in an SA production start-up project in KMEX Silao Plant (Photo 2), which is located 400 kilometers northwest of KMEXDF. I had valuable experiences there including warehouse arrangement, consideration for physical distribution, and completion of initial inventory. It is needless to say that these experiences drove my motivation for working in Marketing for the Latin American market later.

Photo 2 KMEX Silao Plant

After that, I also served as Latin America Sales Manager between 2018 and 2022. During that period I traveled across 15 countries in the Central and South American continent, trying to sell our products to local markets. In Central and South America, people speak Spanish in all the countries including Argentina in the south except for Brazil (and some English-speaking Caribbean countries). People of various origins including Spain, Africa, and indigenous have different business practices and national characteristics. I discussed business with local customers while learning Spanish to gain a lot of experience, although I actually had difficulty in negotiating with those diverse people.

A big challenge during marketing was to protect (and expand) the KYB share in the market from inexpensive Chinese products that were quickly extending their reach. Prioritizing commercially available products, I took various actions.

In fact, inexpensive products were flooding most of the Latin American markets to drive down the market price. At the time, our sales promotion had already reached a plateau several years earlier. To overcome the situation, we put made-in-Mexico products in the market at competitive prices under the slogan of "local production for local consumption". We also focused on sales promotion of the K'lassic brand (low-priced products for older-model cars).

One thing that was very difficult was that most markets in Central and South America preferred made-in-Japan, although it depends on the degree of price difference. They had prejudice or even "allergy" against products made in other countries, which posed barriers to sales promotion of made-in-Mexico products.

As an incentive to overcome the barriers, we invited 14 customers from 10 countries to KMEX Plant for a plant tour (Photo 3). We tried to make them understand that the made-in-Mexico products have the same quality as the

made-in-Japan counterparts as both are produced in an identical total manufacturing system including production processes, materials used, and quality assurance. We also continued our sales promotion campaign. However, I was impatient when these efforts hardly bore any fruit initially.

Photo 3 KMEX Silao Plant tour (Peruvian customers)

We also held an event called KYB Safety Day for which an F1 circuit course in Mexico was rented out to invite customers from 13 countries for testing of various vehicles for comparison. We patiently continued trying to make customers directly feel and understand the KYB quality (Photo 4).

Unexpectedly, the customer demand during fiscal 2021 sharply rose in reaction to the COVID-19 pandemic, resulting in inventory runout at manufacturers and confused physical distribution. Customers tended to purchase as much as available of any products regardless of their origin. We eventually got the sales of made-in-Mexico products on track.

Sales of the low-priced K'lassic series were launched in 2015. Initially, customers hesitated about introducing them due to their rather streamlined specifications or appearance. We enhanced the product line up mainly for low-priced models and gradually expanded the marketing area through sales promotion activities. In fiscal 2021, we eventually expanded the marketing area to the total KMEX territory.

Photo 4 KYB Safety Day

4. Mexican Food and Liquor

As I said earlier, a full lineup of food from all over the world is available in Mexico City though not at reasonable prices. I seldom had a hard time to find a good place to eat. Mexican cuisine, which is registered in the UNESCO Lists of Intangible Cultural Heritage, provides a wide choice of options and is very delicious even to the Japanese.

The staple food in Mexico is basically corn. Tacos (Photo 6) are a typical Mexican food consisting of a corn- or wheat-based tortilla topped with a filling of meat, fish, vegetables, and salsa (sauce). Each region in the country has its own way of enjoying tacos. Anyway it is common practice for the Mexicans to finish off a night of drinking with a taco just like Japanese do with ramen.

Photo 5 Taco restaurant

Photo 6 Tacos

Mexican liquors are also abundant in type. Corona beer is very famous in Japan too. Besides that, you can enjoy a variety of tasty beer from light ones to robust craft beer.

When you think of Mexico, the first thing that comes to mind may be tequila. Various types of tequila are sold by various brands. There are different classes of tequila from "blanco" (white), and "reposado" to "añejo" (ultra-aged) according to the maturation time, as in "junmai" (pure rice), "ginjo" (special brew) and "daiginjo" (very special brew) of Japanese sake. It is interesting to try different classes of tequila for comparison.

Tequila originated in the colonial age in the 16th century. Tequila was born when a Spanish colonist tried to make an alcoholic beverage using a local plant named agave. The village of Tequila exists in the State of Jalisco in Mexico. Only product produced around the village of Tequila can be called tequila.

Photo 7 Tequila and mescal

Another alcoholic beverage that is a little more special is mescal. This liquor is produced from the same ingredients as those of tequila but uses more types of ingredient and more production processes. Bulbs of agave (Photo 8) are buried under the ground and steamed for long hours to give a smoky flavor, which is similar to that of very peaty Scotch whisky.

The production processes of both tequila and mescal have been traditionally passed down over several hundreds of years. You can spend precious time recalling the history and tradition cultivated in each distiller.

Photo 8 Agave - Raw material of tequila and mescal

5. World Heritage and Sightseeing in Mexico

One of the joys for expatriates is travelling in the country and its adjacent areas. In Mexico, the tourism industry is the third biggest source of foreign earnings. It's no exaggeration to say that tourism is an engine for the Mexican economy.

That is why the Mexican government continued accepting foreign tourists through borders kept open without tightening immigration control even during the COVID-19 pandemic in 2020.

Moreover, Mexico is positioned as an entry gate to Latin America and is teeming with tourists throughout the year. The country is abundant in sightseeing spots from pyramids still reflecting the once prosperous ancient Maya and Aztec civilizations (Photo 9), Cancun, which is a world-famous beach facing the beautiful turquoise blue ocean in the Caribbean Gulf (Photo 10), to Acapulco and Los Cabos on the Pacific coast. All these places are not-to-be-missed spots for tourists travelling in Mexico.

Photo 9 Pyramid of the Moon viewed from the top of Pyramid of the Sun

To visit these tourist spots from Mexico City which is located inland, you have to take a flight. Still, any of these spots are easily accessible with just a two hour or so domestic flight. I often travelled to Cancun and fully enjoyed fishing and marine sports there.

Photo 10 Cancun

Another popular tourist amusement in Mexico is winery tours (Photo 11). Wine making is carried out in 14 states of Mexico. The largest producers are wineries in Guadalupe located in Baja California Peninsula. These wineries collectively produce 17 million bottles of wine every year, which is 60% of the domestic production.

Speaking of wine in the American continent, Chile and Argentina are famous producers. In fact, Mexico has the longest history of wine making throughout the continent. The country has continued wine making for over 400 years since the technique was introduced from Spain in the 16th century.

Mexico is warm and dry in climate with a substantial difference in temperature between day and night. This climate is the best for grapes to grow. Consequently, the

country produces many varieties of wine including Cabernet Sauvignon, Merlot, and Shiraz. So, a variety of tasty, high-cost performance wines are available in the country.

Photo 11 Winery

Guadalupe has a famous wine road where a number of wineries stand side by side. Tourists can visit these wineries to join a winery tour to taste wine and learn their wine making processes.

In addition, there are a lot of restaurants that serve dishes of locally-produced cheese and local specialties. You can join a tour to visit three or more such restaurants, spending a happy holiday.

Baja California Peninsula, which is located south of California State in the U.S., is a very popular tourist place along with Cancun.

In this slender peninsula, sandwiched between the Pacific Ocean to the west and the Gulf of California to the east, cultivation of tuna and other marine products is actively conducted. You can eat fatty tuna, fresh sea urchin, abalone, and other premium marine products with great relish.

6. In Closing

I finished my seven-year assignment in Mexico thanks to warm-hearted support from my supervisors, other expatriates, local staff, and my family. I would like to take this opportunity to express my appreciation and say thanks to all these people. I believe that my experience and personal contacts accumulated during the assignment will give me much sustenance and confidence to carry out my future work. I greatly appreciate that I was given this valuable opportunity.

Compañeros, gracias a sus amables apoyos que me han brindados durante 7 años, pude cumplir el reto que tenia en Mexico exitosamente.

Era mi gran orgullo por haber trabajado con ustedes y esta experiencia sera mi gran confianza para seguir trabajar en KYB ahora en adelante.

Muchas gracias!

Saludos,

Author

KAWAI Hiroshi

Joined the company in 2013.
Commercial Product Sales Sect.
No.1, Global Marketing Promotion Dept., Marketing Div.
Took present post after working in Product Planning Sect. of Commercial Product Headquarters, working in Commercial Product Sales Div., and as expatriate at KYB Mexico DF branch.

Glossary

Hard Chrome Plating

Refer to “Making Plating Thickness Constant by Simulation” (page 3)

MOCHIZUKI Yoshitaka
R&D Sect. No.1, Production Technology R&D Center, Engineering Div.

1 What is Plating?

Plating is a technique to provide the target material with additional surface properties that the material does not have itself. Plating is conducted to impart one or more of the following three major properties:

① Corrosion resistance plating
To prevent corrosion of the material
(Example) Galvanizing: Galvanized sheet roof

② Decorative plating
To improve the appearance
(Example) Decorative chromium plating:
Automotive emblems

③ Functional plating
To impart wear resistance, electrical properties, heat resistance, or other properties
(Example) Hard chrome plating: Sliding parts

2 What is Hard Chrome Plating?

The main constituent of hard chrome plating is chromium trioxide (CrO_3). The plating uses a bath containing a minute amount of sulfuric acid as catalyst. As shown in Fig. 1, an object to be plated (work) is put in the plating bath as the cathode while a lead alloy electrode is used as the anode. When they are energized, chrome metal is deposited on the work.

The plating film (chrome metal) obtained in this way is generally applied to sliding parts of machinery, molding dies, rolls for papermaking, and other various components and shows the following characteristics:

- Rust-proof, metallic luster in normal environments
- Hard coating (800 to 1,000 HV - about three times harder than iron)
- A low coefficient of dynamic friction

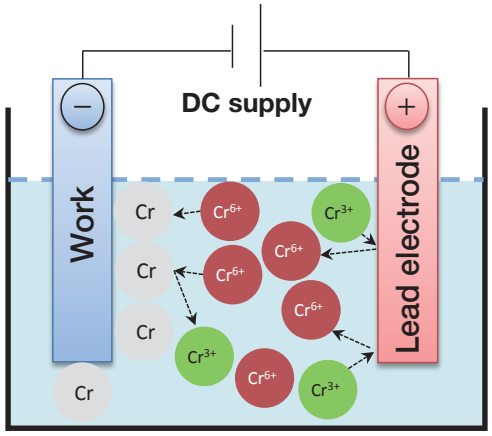

Fig. 1 Chrome plating system

3 Applications of Hard Chrome Plating in KYB

KYB applies hard chrome plating to piston rods of shock absorbers for four-wheel vehicles (Photo 1) and hydraulic cylinders mainly for the purpose of improving corrosion resistance, wear resistance, or sliding characteristics.

Photo 1 Chrome plated product

Glossary

Compensators in Control Systems

Refer to “Control Technologies for In-Vehicle Electric Actuators” (page 8)

MATSUMOTO Daisuke
Development Sect. No.2, Electronics Technology Dept., Engineering Headquarters,
Automotive Components Operations

1 What is a Compensator?

1.1 Role of Compensators

The compensator Note 1) in a control system refers to a component that generates manipulated variables (control input) to attain a desirable response (control output) from the system.

Note 1) This document uses the term “compensator”, not the term “controller” which may sometimes be used.

As an example, a case is considered in which a vehicle is applied with a driving force u (control input) and controlled so that its velocity v (control output) is maintained at a fixed target velocity v_r (setting value) (Fig. 1). The vehicle is affected by disturbances d such as aerodynamic drag, friction against the road surface, and forces caused by gravity on slopes. It is assumed here that disturbances d are almost constant.

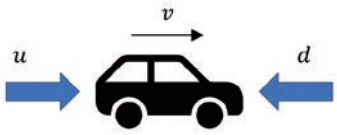

Fig. 1 Vehicle velocity control

Then, a control system is configured as shown in Fig. 2:

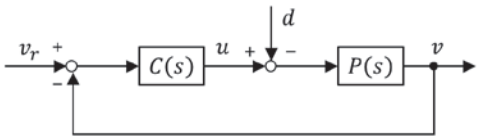

Fig. 2 Vehicle velocity control system (1)

where

$P(s)$: Transfer function of controlled object (transfer function from the force applied to the vehicle u-d to the velocity v)

$C(s)$: Transfer function of compensator

s: Laplace operator (or differential operator)

For the control system in Fig. 1, the velocity v of the vehicle can be expressed by the equation below:

$$v = \frac{C(s)P(s)}{1+C(s)P(s)}v_r - \frac{P(s)}{1+C(s)P(s)}d \tag{1}$$

As time elapses ($s \to 0$), the vehicle velocity v can be expressed by the equation below:

$$\begin{aligned} v &= \frac{C(0)P(0)}{1+C(0)P(0)}v_r - \frac{P(0)}{1+C(0)P(0)}d \\ &= \frac{1}{\frac{1}{C(0)P(0)}+1}v_r - \frac{\frac{1}{C(0)}}{\frac{1}{C(0)P(0)}+1}d \end{aligned} \tag{2}$$

When the compensator $C(s)$ is designed so that $C(0)$ is sufficiently large, $1/C(0)$ in Eq. (2) is almost zero (0). The vehicle velocity v is almost $v = v_r$ accordingly. Designing the compensator $C(s)$ in this way will achieve one of the control objectives, that is, “to keep the velocity close to the target value”. Behind the control objectives lie a wide range of needs including cost-effectiveness, safety, and comfort. The role to be played by the compensator in order to satisfy these needs will be described in Chapter 3.

1.2 Types of Compensators and Example of Control System Characteristics

Typical compensators include proportional, differential, integral, phase lead, and phase lag compensators. A detailed description of these compensators is omitted here.

To achieve one of the control objectives “to keep the velocity close to the target value” stated in the previous section, a proportional and integral compensator will be sufficient, provided that the transfer function of the controlled object can be expressed by the equation below:

$$P(s) = \frac{1}{Ms} \tag{3}$$

where M indicates the weight [kg] of the vehicle. Eq. (4) represents an ideal vehicle that is applied with a control

input u without delay. The transfer function of the proportional and integral compensator can be expressed by the equation below:

$$C(s) = K_P + \frac{K_I}{s} = \frac{K_P s + K_I}{s} \tag{4}$$

where K_P and K_I are proportional and integral gains, respectively. When Eqs. (3) and (4) are substituted in Eq. (1), the vehicle velocity v can be expressed by the equation below:

$$\begin{aligned} v &= \frac{C(s)P(s)}{1+C(s)P(s)} v_r - \frac{P(s)}{1+C(s)P(s)} d \\ &= \frac{\frac{K_P}{M} s + \frac{K_I}{M}}{s^2 + \frac{K_P}{M} s + \frac{K_I}{M}} v_r - \frac{\frac{1}{M} s}{s^2 + \frac{K_P}{M} s + \frac{K_I}{M}} d \\ &= \frac{2\zeta\omega_n s + \omega_n^2}{s^2 + 2\zeta\omega_n s + \omega_n^2} v_r - \frac{\frac{1}{M} s}{s^2 + 2\zeta\omega_n s + \omega_n^2} d \end{aligned} \tag{5}$$

where

$$\omega_n = \sqrt{K_I/M},\ \zeta = K_P\sqrt{1/(K_I M)}/2$$

Setting K_P and K_I to achieve $0 < \omega_n$ and $0 < \zeta$ will make the control system stable. The equation also implies that, as time elapses ($s \to 0$), $v = v_r$ will hold.

1.3 How to Configure Compensators

There are two types of compensator configuration: analog and digital. An analog compensator uses resistors, capacitors, operational amplifiers, and other elements. The example shown in the previous section assumes control with an analog compensator. The transfer function of an analog compensator is represented using the Laplace operator s (or differential operator). A digital compensator is configured using a logic circuit or digital computer. Digital compensators have the advantage that complex compensators can be configured using software, thereby enabling the user to easily modify parameter settings. Today, many control systems for in-vehicle actuators use digital compensators because the performance of microprocessors has been improved. The transfer function of a digital compensator is represented using the z and δ operators.

2 Parametrization of Stabilizing Compensators

Parametrization of stabilizing compensators was proposed by Youla and others during the 1970s [1]. This may be called "Youla parametrization". Studies on robust control theory became active toward the 1990s and many books explaining how to apply Youla parametrization to actual control scenes [2] were published. A stabilizing compensator design with parametrization should represent "how the compensator should be" derived from a model of the controlled object and the desirable characteristics of the control system, instead of "first selecting the type of the compensator", such as proportional or integral as introduced in section 1.2, before designing. In other words, the designer can find a compensator satisfying the desirable characteristics of the control system even if the controlled object is quite complex. Still, a more-or-less accurate model of the controlled object (a mathematical model such as transfer function) will be needed. In some cases, the achievable characteristics of the control system may be limited depending on the characteristics of the controlled object. For your information, the proportional and integral compensator stated in section 1.2 can also be derived from the parametrization of a stabilizing compensator.

3 Two-degree-of-freedom Control System

The control system described in Chapter 1 may have other control objectives than just "to keep the velocity close to the target value", attributable to various demands including "[1] to reduce the fuel (or electricity for electric vehicles) consumption during acceleration (cost-effectiveness)", "[2] to reduce the shock felt by passengers during acceleration or deceleration (ride comfort)", and "[3] to minimize speed variations during driving on slopes (safety)". Demands [1] and [2] mainly relate to target tracking and [3] relates to disturbance response. With a focus on Eq. (1) in section 1.1, target tracking (the first term on the right-hand side) and disturbance response (the second term on the right-hand side) are both decided by the compensator $C(s)$. This means that, in some cases, demands [1] & [2] and demand [3] can hardly all be satisfied at the same time. Then, another control system should be considered as shown in Fig. 3:

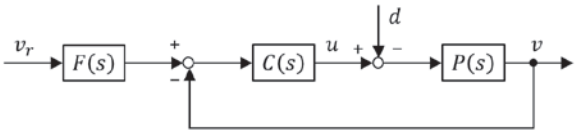

Fig. 3 Vehicle velocity control system (2)

The velocity v of the vehicle with the control system in Fig. 3 can be expressed by the equation below:

$$v = \frac{F(s)C(s)P(s)}{1+C(s)P(s)} v_r - \frac{P(s)}{1+C(s)P(s)} d \tag{6}$$

With an additional compensator $F(s)$, target tracking (the first term on the right-hand side) and disturbance response (the second term on the right-hand side) can be set separately. That is, two-degree-of-freedom design is now available. In this sense, the control system in Fig. 3 is called a two-degree-of-freedom control system.

References

1) D.C. Youla, Hamid A. Jabr, J.J. Bongiorno Jr: Modern Wiener-Hopf Design of Optimal Controllers - Part II: The Multivariable Case, IEEE Trans. Auto Control, AC-21, No. 3, pp. 319-338, (1976).

2) MAEDA, SUGIE: System Control Theory for Advanced Control, Asakura Publishing, (1990).

Glossary

PV Values of Vane Pumps

Refer to “Development of Vane Pump for Medium Passenger Vehicle CVT” (page 26)

HAGIWARA Takahiro
Pump Engineering Dept., Steering Business Dept., Automotive Components Operations

1 What is the PV Value?

The PV value (or PV factor) is one of the wear factors in a sliding scene and can be calculated from the pressure (P) applied to the contact surfaces of the sliding parts and the sliding velocity (V).

The surface pressure P can be determined by dividing the pressing force N by the contact area A.

2 PV Value of Vane Pumps

2.1 Operating Principle of Vane Pumps

First of all, the following describes the pumping mechanism of vane pumps to suck or discharge the hydraulic oil:

① The engine outputs a driving force to rotate the rotor of the pump via the shaft.
② As the rotor rotates, vanes inserted in the slots pop up radially with the centrifugal force and the pump’s internal pressure increase on the back of the vanes.
③ The pop-up vanes slide along the curved internal surface (oval shape) of the cam ring.
④ The pump sucks or discharges the oil as the oil chamber formed by the cam ring, rotor and vanes increases or decreases in volume.

These parts and their operation are shown in Fig. 1.

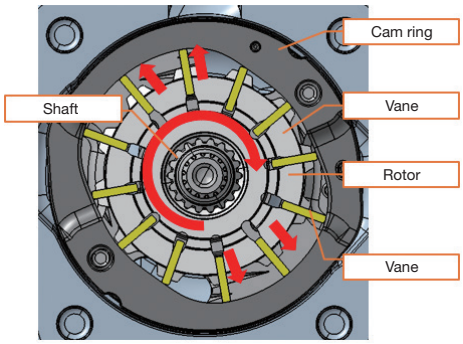

Fig. 1 Cross section of vane pump

2.2 PV Value of Vane Pumps

As the rotor rotates, the pop-up vanes are pressed against the cam ring by the centrifugal force and the pump’s internal pressure increase on the back of the vanes. This applies the surface pressure P to the contact surfaces. The vanes slide along the cam ring surface at a sliding velocity V as the rotor rotates.

A lower PV value implies higher wear resistance and a higher PV value brings about lower wear resistance. The PV value at which the cam ring wears out is called the PV limit. Photo 1 shows a cam ring that was subjected to a durability test with a PV value exceeding the PV limit and eventually worn out. Photo 2 shows a cam ring that was subjected to a durability test with a PV value lower than the PV limit.

To improve the wear resistance of a vane pump, the PV value should be kept at a low level. To do so, the surface pressure P must be reduced by increasing the contact area A, decreasing the pressing force N, or lowering the sliding velocity V.

Wear resistance is affected not only by the PV value but also by material, surface roughness, and hardness of the parts coming into contact with each other, lubrication of the hydraulic oil, and other factors. It is necessary to design a vane pump with considerations given to the balance among these factors.

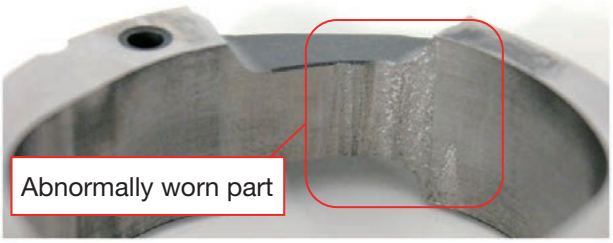

Photo 1 Abnormally worn cam ring with PV value exceeding the limit

Photo 2 Cam ring with PV value lower than the limit after durability test

Editors Script

I have long been involved in research and development. For me, KYB Technical Review is a stage from which to advertise the results of engineering and product development efforts to the external world. Article auditors can leave the resulting technologies here as a record to be handed down to posterity. As an engineer, I am honored to be one of the contributors to the Review. Since it is difficult to publish sensitive information about, for example, products under development or knowhow related to production engineering, the Review might not provide readers with sufficient information at this moment. For compiling articles in the future, we need to fully consider what information readers may find useful. Then, we would like to introduce technologies and products that are commonly known internally but might be novel to readers. (SAITO)

I definitely think it is difficult to explain something to others that is unknown to them. Words that are used among one group of people in a casual way often cannot be understood by another group of people. Basically, others do not listen to your words from a speaker's position. I always find the text in the articles of KYB Technical Review easy to understand. I really respect contributors to the Review who respond to me amiably when I visit their place to urge them to finish their script even when they are busy. Thanks to them, I, as an editorial member, have been able to help continue publishing this issue. If possible, I wanted to buy them a glass of beer and say, "you did it", but that was difficult under the current situation. I seriously hope that various controls related to COVID-19 will be lifted soon. (SASAKI)

I have been involved in editing KYB Technical Review for the first time after a change of editors. I had once contributed to the Review but had never joined the editorial team. Now I am able to understand how the editors are working hard behind the scenes on a publication that I had been reading without noticing them. The Mie district that I am in charge of has not yet come up with a new research and development achievement, so I have had little chance of helping our engineers contribute to the Review. I am now part of the editorial team of the Review, which is one of the media to publish research and development being steadily carried out at other sites. As an editorial member, I will do my best to support contributors and other editors in any way I can. (YONEKAWA)

KAYABA TECHNICAL REVIEW No.65

Published on October 1, 2022
Editor and Publisher: KAYABA Technical Review Editorial Board
Publishing Office: KYB Corporation
(KYB Corporation adopted the common name of KAYABA Corporation on April 1, 2022).
World Trade Center Building South Tower 28F, 2-4-1 Hamamatsu-cho, Minato-ku, Tokyo 105-5128, Japan
Tel: 03-3435-3511
Fax: 03-3436-6759
Published by Shobi Printing Co., Ltd. (Hakusan, Tokyo)

Notification regarding website release

Thank you for supporting KAYABA TECHNICAL REVIEW. Since the 50th edition (issued in April 2015), we have been releasing these reviews on our website with the aim of enabling more people to read them.
We will also continue to publish the booklets as usual, so please read the printed version and/or the website at your convenience.

<KYB website>
https://www.kyb.co.jp/
(Please click on the KYB REVIEW banner on the home page).